US-Ukraine Quantum Forum 2023

Conference Proceedings

October, 2023

Contents

Organizers

- Denys Bondar, Tulane University, USA

- Andrii Sotnikov, NSC KIPT and V.N. Karazin National University, Kharkiv, Ukraine

Confirmed Invited Speakers

- Maija Kukla, Program Director, OISE/OD/NSF "*DCL: IMPRESS-U. International Multilateral Partnerships for Resilient Education and Science System in Ukraine*".

- Martina Barnas, Office of Naval Research Global, London, UK,
  Jonathon Brame, Engineer at Engineer Research and Development Center, US Army,
  Charlton David Lewis, Program manager in the Defense Sciences Office, DARPA
  ''*Partners in Science. Basic and Applied Research Collaboration Overview*".

- Ignacio Franco, University of Rochester "*Light Field Control of Real and Virtual Charge Carriers*".

- Christian Arenz, Arizona State University "*Speeding up quantum dynamics through local parametric controls*".

- Alexander Burin, Tulane Univeristy "*Many body localization (MBL) in the presence of a long-range interaction. Similarities and differences with Anderson localization and short range MBL problems*".

- Sebastian Deffner, University of Maryland, Baltimore County "*Quantum Stochastic Thermodynamics of Relativistic Systems*".

- Dmitry Lyakh, NVIDIA Corporation "*Accelerating Quantum Science via Efficient HPC Math Libraries and GPU Computing*".

- Dimitris Giannakis, Dartmouth College "*Quantum Information and Data Science for Simulation of Classical Dynamics*".

- Adam Kaufman, JILA, University of Colorado at Boulder "*Microscopically-controlled arrays of alkaline-earth atoms*".

- Mikhail Lukin, Harvard University "*Programmable Quantum Systems based on Neutral Atom Arrays*"

- Alexandra Boltasseva, Purdue University "*The Crossroads of Machine Learning and Nano and Quantum Photonics*".

- Sergey Frolov, University of Pittsburgh "*Fascinating physics in semiconductor-superconductor nanowires*".

- Kurt Jacobs, US Army Research Laboratory and University of Massachusetts, Boston "*Quantum theory of the generation of single-photon nonlinearities by ensembles*".

- Alexei Sokolov, Texas A&M University "*Enhanced Molecular Spectroscopy and Quantum Sensing for Biophotonics*".

- Christopher Fuchs, University of Massachusetts, Boston "*Born's Rule Repainted in a QBist Style*".

- Matt Trusheim, US Army Research Laboratory "*Strongly cavity-coupled solid-state quantum sensors*".

Sponsors

Office of Naval Research Global Grant # N62909-23-1-2088
&
Tulane University, School of Science & Engineering

Forum Webpage

USUAqForum.github.io

Binary ferromagnet-normal metal superlattices
for quantum sensing

Mikhail Belogolovskii[1,2], Ivan Nevirkovets[3]

[1]Kyiv Academic University, Kyiv, Ukraine
[2]Department of Experimental Physics, Faculty of Mathematics, Physics and Informatics,
Comenius University, Bratislava, Slovak Republic
[3]Northwestern University, Evanston, USA

As emphasized in a recent review [1], we are at the dawn of an era of layered quantum materials, which have proven their great potential as scalable components of quantum devices, including nanoscale sensors, and have made it possible to create new quantum phases of matter. In the contribution, we present our results on synthetic binary superlattices formed by nanometer-thick layers of normal and ferromagnetic metals, quantum transport through which unexpectedly demonstrates the formation of edge states, which are resistant to disorder and other mobile charge interactions. The idea of the experiments was inspired by a paradigmatic explanation of the plateaus in transversal transport characteristics of 2D conductors at very low temperatures and strong magnetic fields (the integer quantum Hall effect) that is based on the existence of narrow near-boundary quantum channels of non-interacting electrons created at the Fermi level in strongly disordered electron systems [2]. The edge states are chiral in the sense that they can carry current only in one fixed direction. At the same time, they are topologically protected and their number cannot vary under continuous transformation of the system. This approach assumes the presence of a disordered and isotropic two-dimensional electron gas. Our aim was to create a strongly anisotropic 3D system with edge channels concentrated mainly at the hinges of the structure, i.e., a synthetic material with one or two 1D conducting modes.

The anisotropy in our samples is arising due to the layered structure where the diffusion coefficient for the charge motion across metallic layers ($D_\perp$) is much smaller than that along them ($D_\parallel$). In this case, the dephasing effect is characterized by the average $\langle \exp(-i\phi) \rangle$ of the phase factor ϕ calculated along all diffusive paths. If the related point belongs to the central region of the sample, a huge number of contributions with random signs largely cancel each other yielding $\langle \exp(-i\phi) \rangle$ to be proportional to $\exp(-d^2/l_B^2)$ with $l_B^2 = \Phi_0/\sqrt{D_\parallel/D_\perp}B$; here, Φ_0 is the magnetic flux quantum, and B is the magnetic flux density within the superlattice. In contrast to the central part of the superlattice, the presence of a nearby boundary imposes a sharp geometrical constraint on the allowed paths and near-surface trajectories are surviving. This is even more appropriate for 1D hinge states localized at the intersection of two surfaces. The presence of two hinge states at opposite edges of the superlattice can induce beats between their contributions.

However, the disorder factor is insufficient to guarantee the chirality of the edge states in the absence of the magnetic field or in the presence of a very weak field. For this, a source of the internally broken time-reversal symmetry is needed. It can be realized in a magnetically frustrated system where scattering off from spin clusters can generate an enhanced skew (asymmetric) scattering potential, one of the major mechanisms causing anomalous Hall effect in the absence of the magnetic field, and even without the spin-orbit interaction [3]. Hence, combination of the two

factors – hinge states surviving in the strongly disordered and anisotropic material and the skew scattering by small ferromagnetic nanoparticles – can generate the chiral edge currents.

One of the best ways to probe spatial current distributions is Josephson interferometry in a stacked (layered) configuration where the hybrid structure under study links two superconducting (S) electrodes. The figure of merit in such experiments is the maximum supercurrent (I_c) versus in-plane magnetic field (H). In our experiments, we applied this technique to study the transport of Cooper pairs through a periodic multilayer formed by ten normal metal (Al) - ferromagnetic metal (Ni or Ni-Fe alloy) bilayers. For the first time, we observed SQUID-like ($I_c(H)$) oscillations instead of conventional Fraunhofer patterns expected for trivial S-weak link-S junctions. Multilayers were deposited in situ by DC magnetron sputtering of the respective materials onto oxidized Si substrates at room temperature. The multilayered Josephson junctions were patterned using optical lithography, reactive ion etching, Ar ion milling, and anodization followed by deposition of additional SiO_2 insulation. Our first experimental results on the multilayered samples can be found in the publications [4,5].

Using $I_c(H)$ characteristics for $S(NF)_{10}NI(NF)_{10}NS$ samples, we reconstructed the supercurrent-density spatial dependence. In chiral channels, an electron propagating along the interface with a superconductor could be reflected as a hole moving in the same chiral direction, then reflected as an electron and so on. Such combination of Andreev reflections with the chiral motion yields chiral Andreev edge states transferring superconducting correlations between S electrodes. We have found that the transport channels are strongly asymmetric with respect to the weak-link center and possibly one-dimensional. The strong asymmetry reveals itself also in the prominent upward shift of the periodic $I_c(H)$ curves while the amazing survival of edge transport in spite of the numerous scatterings at the boundaries of the neighboring layers remains unclear and may suggest a topological nature of the near-surface modes. The two important results, at overwhelming contribution of the supercurrent unidirectional motion inside the multilayer and the double period of $I_c(H)$ oscillations, may point to the realization of chiral Andreev edge states in the samples studied. Additional evidence in favor of this assumption would be direct observation of specific Andreev scattering, in which an electron propagating along the interface of the hybrid $(NF)_n$ multilayer with a superconducting film can be Andreev-reflected only as a hole flowing in the same chiral direction, see above.

For this purpose, we fabricated new samples with an additional SIS junction playing the role of a "bottleneck" inside the weak link and thus controlling the current flowing through the whole heterostructure. Strong hysteresis in the current-voltage curves and its virtual absence in $S(NF)_{10}NI$-$(NF)_{10}NS$ miltilayers confirms the dominance of charge transfer through the SIS contact. By measuring its dependence on an external in-plane magnetic field, we could verify whether the supercurrent flows through the SIS junction along its edges, as it would be in the case of helical states, or it flows across the entire junction that would be a transport signature of chiral Andreev edge currents. Pursuing this goal, we replaced one of the outside S electrodes in the $S(NF)_{10}NS$ heterostructure with a conventional Josephson $Nb/Al/AlO_x/Al/Nb$ (SNINS) junction. Comparing the Fraunhofer pattern in such devices with those measured for conventional ones, we can see that the supercurrent distribution over the outside S film is fairly uniform. The remaining asymmetry leads to the absence of nodes in the Fraunhofer-like pattern and lack of strict periodicity of the minima. Since the scattering probabilities at corners of the interface between the weak-link edges

and an S electrode strongly depend on their geometries, the values of the critical current in such configuration are small and highly variable.

In the second type of heterostructures, an I interlayer in the $S(NF)_{10}NI(NF)_{10}NS$ mulilayers discussed above was replaced with an SNINS junction. In this configuration, the internal Josephson SNINS junction is placed between two $(NF)_{10}N$ multilayers. We have found that the main period of the diffraction pattern in such samples is determined by the SNINS junction parameters, whereas small-amplitude "ripples" observed in experimental $I_c(H)$ curves are associated with the presence and properties of the $(NF)_{10}N$ multilayers. The principal dissimilarity with the previous samples is that the two magnetic $(NF)_{10}N$ subsystems are separated by a superconducting junction shielding their mutual interaction and weakening magnetic exchange coupling, allowing thus various orientations of the magnetizations. As a rule, in multilayered systems similar to ours, an out-of-plane magnetic anisotropy is observed. Tunnel junction with a very thin oxide barrier and magnetic electrodes formed by perpendicularly magnetized films usually display their antiferromagnetic coupling, whereas similar structures with in-plane magnetized electrodes exhibit conventional ferromagnetic coupling. Nevertheless, when the spacer is a superconducting film, the coupling of ferromagnetic layers via superconducting current induces antiferromagnetic-like interaction between them.

Resuming, we would like to emphasize that unidirectional and backscatter-free propagation of charge carriers in three-dimensional materials is of fundamental interest in physics and high demand for quantum technologies thanks to possibility of novel excitations like chiral Majorana fermions. In this regard, great hopes are associated with the implementation of higher-order topological insulators characterized by hinge states protected by various spatiotemporal symmetries. In the work, we demonstrate signatures of such non-trivial edge modes in stacked binary multilayers formed by conventional normal and magnetic nm-thick metallic films placed between two superconducting electrodes. Our main findings are as follows:

- The emergence of non-trivial edge transport modes occurs in $(NF)_n N$ multilayers with a sufficiently large number n of bilayers. Despite a huge number of electronically mismatched interfaces and the presence of magnetic nanoparticles (most probably, in a superparamagnetic regime) the phase-coherent charge transport stays quantum.

- The bulk of the $(NF)_n N$ weak link is not involved in the transfer of Cooper pairs between two superconducting Nb electrodes. It is carried out via Andreev bound states localized near the edges of the $(NF)_n N$ periodic structure. If we take into account the sizes of only this region, the values of superconducting critical parameters match those for highest-quality SIS Josephson junctions made with conventional niobium technology.

- Permanent observation of a single (sometimes two) period in the critical supercurrent I_c versus probing in-plane magnetic field H patterns indicates quasi-one-dimensional nature of the near-edge current(s) which are mostly unidirectional with a small part of oppositely moving quasiparticles.

References

1. A. R.-P. Montblanch et al. Layered materials as a platform for quantum technologies, Nat. Nanotechnol. **18**, 555 (2023).

2. R. A. Romer and J. Oswald. The microscopic picture of the integer quantum Hall regime. Ann. Phys. **435**, 168541 (2021).

3. Y. Fujishiro et al. Giant anomalous Hall effect from spin-chirality scattering in a chiral magnet. Nat. Commun. **12**, 317 (2021).

4. I. P. Nevirkovets, M. A. Belogolovskii, and J. B. Ketterson. Josephson junctions with artificial superparamagnetic barrier: a promising avenue for nanoscale magnetometry. Phys. Rev. Applied **14**, 014092 (2020).

5. I. P. Nevirkovets, M. A. Belogolovskii, O. A. Mukhanov, and J. B. Ketterson. Magnetic field sensor based on a single Josephson junction with a multilayer ferromagnet/normal metal barrier. IEEE Trans. Appl. Supercond. **31**, 9343682 (2021)..

Towards the problem of propagation of correlations in open systems

Igor Gapyak

Taras Shevchenko National University of Kyiv, Kyiv, Ukraine

One of the challenging problems of the theory of open quantum systems consists in the rigorous derivation of the master kinetic equation with initial correlations, that is, a quantum kinetic Fokker-Planck type equation, which takes into account the evolution of initial correlations, from the dynamics of many particles. The solution to this problem, in particular, is related to the question of the mechanism of stochastic behavior in dynamic systems of many particles.

Recently, in particular, when studying applied issues related to the propagation of correlations between the system and environment, the problems of the dynamics of the initially correlated open quantum systems began to be investigated systems. This work is devoted to a mathematical derivation of the quantum kinetic equation for a traced particle, with initial correlations between the traced particle and the environment. Such a traced particle can be characterized by a different mass or a special potential for interaction with the environment. Initial correlations between states refer to situations where the quantum states of a composite system are correlated with each other at the beginning of a quantum process. These correlations can arise from previous interactions or preparations of the subsystems. In a number of works that investigate quantum computing and quantum technologies, taking into account the initial correlations between the isolated quantum subsystem and the quantum environment is of crucial importance.

In modern works, the main approach to the study of the collective behavior of open systems consists in the construction of scaling approximations, for example, the diffusion limit, for the solution of evolution equations that describe the evolution of the state of a system of many particles, which consists of a traced particle in the environment of many particles. For a system with an infinite number of particles, this is a perturbative solution of the BBGKY (Bogolyubov–Born–Green–Kirkwood–Yvon) hierarchy for open systems.

In the talk, based on the non-perturbative solution of the BBGKY hierarchy for the reduced density operators of an open quantum system, a new approach to the rigorous derivation of the Fokker–Planck type kinetic equation with initial correlations is proposed. In particular, this approach makes it possible to describe the process of propagation of initial correlations in open quantum systems.

Let the n-particle space $\mathscr{H}_n = \mathscr{H}^{\otimes n}$ is a tensor product of n Hilbert spaces $\mathscr{H}$ and $\mathscr{H}_0 = \mathbb{C}$. We denote $\mathscr{F}_{\mathscr{H}} = \oplus_{n=0}^{\infty} \mathscr{H}_1 \otimes \mathscr{H}_n$ the Fock space. Let $\mathfrak{L}_{\alpha}^1(\mathscr{F}_{\mathscr{H}})$ be the space of sequences $f = (f_0, f_{1+0}, f_{1+1}, \ldots, f_{1+n}, \ldots)$ of trace class operators $f_{1+n} \equiv f_{1+n}(\mathfrak{t}, 1, \ldots, n) \in \mathfrak{L}^1(\mathscr{H}_1 \otimes \mathscr{H}_n)$ and $f_0 \in \mathbb{C}$ and for arbitrary $(i_1, \ldots, i_n) \in (1, \ldots, n)$ they satisfy the symmetry condition: $f_{1+n}(\mathfrak{t}, 1, \ldots, n) = f_{1+n}(\mathfrak{t}, i_1, \ldots, i_n)$, and are equipped with the norm:

$$\big\| f \big\|_{\mathfrak{L}_{\alpha}^1(\mathscr{F}_{\mathscr{H}})} = \sup_{n \geq 0} \alpha^{-n} \mathrm{Tr}_{\mathfrak{t}, 1, \ldots, n} \big| f_{1+n}(\mathfrak{t}, 1, \ldots, n) \big|,$$

where $\mathrm{Tr}_{t,1,\dots,n}$ are partial traces and the parameter $\alpha > 0$ is a real number. Let $\mathfrak{L}_0^1 \in \mathfrak{L}_\alpha^1(\mathscr{F}_{\mathscr{H}})$ be the subset of finite sequences of degenerate operators with infinitely differentiable kernels with compact supports.

The evolution of all possible states of an open quantum system is described by the sequences $F(t) = (F_{1+0}(t,\mathsf{t}), F_{1+1}(t,\mathsf{t},1),\dots,F_{1+s}(t,\mathsf{t},1,\dots,s),\dots) \in F_{\mathscr{H}} \in \mathfrak{L}_\alpha^1(\mathscr{F}_{\mathscr{H}})$ of reduced density operators, which are a non-perturbative solution of the Cauchy problem for the quantum BBGKY hierarchy:

$$F_{1+s}(t,\mathsf{t},1,\dots,s) = \sum_{n=0}^{\infty} \frac{1}{n!} \mathrm{Tr}_{s+1,\dots,s+n} \, \mathfrak{A}_{1+n}(t,\{\mathsf{t},1,\dots,s\}, \tag{2.1}$$
$$s+1,\dots,s+n) F_{1+s+n}^0(t,1,\dots,s+n), \quad s \geq 0.$$

The generating operator of the n-th term of the series (2.1) is determined by the cumulant of the $(n+1)$-th order one-parameter group of operators:

$$\mathfrak{A}_{1+n}(t,\{\mathsf{t},1,\dots,s\},s+1,\dots,s+n) =$$
$$\sum_{\mathrm{P}:\,(\{\mathsf{t},1,\dots,s\},s+1,\dots,s+n)=\bigcup_i X_i} (-1)^{|\mathrm{P}|-1}(|\mathrm{P}|-1)! \prod_{X_i \subset \mathrm{P}} \mathscr{G}_{|\theta(X_i)|}^*(t,\theta(X_i)),$$

where $\sum_P$ means the sum over all possible partitions P of the set $(\{\mathsf{t},1,\dots,n\},s+1,\dots,s+n)$ on $|P|$ nonempty subsets $X_i \subset (\{\mathsf{t},1,\dots,n\},s+1,\dots,s+n)$ which do not mutually intersect, the set $\{\mathsf{t},1,\dots,n\}$ consists from one element, that is $|\{\mathsf{t},1,\dots,n\}| = 1$ and the operator θ is the declusterization mapping: $\theta(\{\mathsf{t},1,\dots,n\}) = (\mathsf{t},1,\dots,n)$. On the space of trace class operators $\mathfrak{L}^1(\mathscr{H}_1 \otimes \mathscr{H}_n)$ is defined one-parameter group of operators:

$$\mathscr{G}_{1+n}^*(t)f_{1+n} \doteq e^{-itH_{1+n}} f_{1+n} e^{itH_{1+n}},$$

where the operator H_{1+n} is the Hamiltonian of the system of the traced particle and n particles of the environment:

$$H_{1+n} = H_{1+0}(\mathsf{t}) \otimes \mathbb{I} + \mathbb{I} \otimes H_{0+\{n\}}(1,\dots,n) + H_{1+\{n\}}(\mathsf{t},1,\dots,n),$$

where $H_{1+0}(\mathsf{t}) = K(\mathsf{t})$ is the operator of the kinetic energy of the traced particle, $H_{1+\{n\}}(\mathsf{t},1,\dots,n) = \sum_{j=1}^n \Phi(\mathsf{t},j)$ is the operator of the pair interaction potential of the traced particle with the environment and $H_{0+\{n\}}(1,\dots,n) = \sum_{j=1}^n K(j) + \sum_{j_1<j_2=1}^n \Phi(j_1,j_2)$ is the Hamiltonian operator of n particles of the environment.

We will consider the initial states of the open quantum system, which are described by a sequence of the following reduced density operators:

$$F_{1+n}(t)_{|t=0} = F_{1+0}^0(\mathsf{t}) F_{0+n}^0(1,\dots,n) g_{1+n}(\mathsf{t},1,\dots,n), \quad n \geq 0, \tag{2.2}$$

where the operator $g_{1+n} \in \mathfrak{L}(\mathscr{H}_1 \otimes \mathscr{H}_n)$ describes the correlations of the states of the traced quantum particle and its environment at the initial moment of time.

Due to the fact that the sequence of initial reduced density operators (2.2) depends on the initial reduced density operator of a traced particle, the Cauchy problem for the corresponding quantum

BBGKY hierarchy is not uniquely defined, so it can be reformulated as a new Cauchy problem for the evolutionary equation for the reduced density operator of the traced particle and a sequence of explicitly defined functionals of the solution of the Cauchy problem of the evolution equation for a one-particle density operator.

Since the initial state of the open quantum system is determined by the initial state of the traced particle (2.2), the state of the system at an arbitrary moment in time (2.1) can also be described in an equivalent way using a sequence of reduced functionals of the state [1-3]:

$$F(t \mid F_1(t)) = (F_{1+0}(t, \mathfrak{t}), F_{1+1}(t, \mathfrak{t}, 1 \mid F_{1+0}(t)), \ldots, F_{1+s}(t, \mathfrak{t}, 1, \ldots, s \mid F_{1+0}(t)), \ldots).$$

The reduced functionals of states $F_{1+s}(t, \mathfrak{t}, 1, \ldots, s \mid F_{1+0}(t))$, $s \geq 1$ are represented by the following expansions in a series:

$$F_{1+s}\big(t, \mathfrak{t}, 1, \ldots, s \mid F_{1+0}(t)\big) \doteq$$
$$\sum_{n=0}^{\infty} \frac{1}{n!} \mathrm{Tr}_{s+1,\ldots,s+n} \, \mathfrak{V}_{1+n}(t, \{\mathfrak{t}, 1, \ldots, s\}, s+1, \ldots, s+n) F_{1+0}(t, \mathfrak{t}), \qquad (2.3)$$

where examples of the first two evolutionary operators $\mathfrak{V}_{1+n}(t)$ are defined by the following expressions:

$$\mathfrak{V}_1(t, \{\mathfrak{t}, 1, \ldots, s\}) = \mathfrak{A}_1(t, \{\mathfrak{t}, 1, \ldots, s\}) F_{0+s}^0(1, \ldots, s) g_{1+s}(\mathfrak{t}, 1, \ldots, s) \mathfrak{A}_1(-t, \mathfrak{t}),$$
$$\mathfrak{V}_2(t, \{\mathfrak{t}, 1, \ldots, s\}, s+1) = \mathfrak{A}_2(t, \{\mathfrak{t}, 1, \ldots, s\}, s+1) F_{0+s+1}^0(1, \ldots, s+1) g_{1+s+1}(\mathfrak{t}, 1, \ldots, s+1)$$
$$\mathfrak{A}_1(-t, \mathfrak{t}) - \mathfrak{A}_1(t, \{\mathfrak{t}, 1, \ldots, s\}) F_{0+s}^0(1, \ldots, s) g_{1+s}(\mathfrak{t}, 1, \ldots, s)$$
$$\mathfrak{A}_1(-t, \mathfrak{t}) \mathfrak{A}_2(t, \mathfrak{t}, s+1) F_{0+1}^0(s+1) g_{1+1}(\mathfrak{t}, s+1) \mathfrak{A}_1(-t, \mathfrak{t}).$$

In general case, the operator $\mathfrak{V}_{1+n}(t)$ is defined in Refs. [1,2].

The one-particle density operator for a traced particle is determined by the Cauchy problem for the quantum Fokker – Planck type equation:

$$\frac{\partial}{\partial t} F_{1+0}(t, \mathfrak{t}) = \mathcal{N}(\mathfrak{t}) F_{1+0}(t, \mathfrak{t}) + \mathrm{Tr}_1 \, \mathcal{N}_{\mathrm{int}}(\mathfrak{t}, 1) F_{1+1}(t, \mathfrak{t}, 1 \mid F_{1+0}(t)), \qquad (2.4)$$

$$F_{1+0}(t, \mathfrak{t})|_{t=0} = F_{1+0}^0(\mathfrak{t}). \qquad (2.5)$$

In equation (2.4), the marginal functional is represented by the expansion in the series (2.3) in the case $s = 1$ and operators $\mathcal{N}(\mathfrak{t})$ and $\mathcal{N}_{\mathrm{int}}(\mathfrak{t}, 1)$ of the von Neumann equation generator are defined on the subspace $\mathfrak{L}_0^1(\mathcal{H}_1 \otimes \mathcal{H}_1)$ according to the following formulas:

$$\mathcal{N}(\mathfrak{t}) f_{1+s} \doteq -i\big(K(\mathfrak{t}) f_{1+s} - f_{1+s} K(\mathfrak{t})\big), \quad \mathcal{N}_{\mathrm{int}}(\mathfrak{t}, 1) f_{1+s} \doteq -i\big(\Phi(\mathfrak{t}, 1) f_{1+s} - f_{1+s} \Phi(\mathfrak{t}, 1)\big).$$

We emphasize that the coefficients of the kinetic equation (2.4) are determined by the initial correlations of the states of the traced particle and its environment.

Thus, if the initial states are determined by a sequence of reduced density operators (2.2), then the evolution of all possible states of an open quantum system can be described without any approximations using the reduced density operator of a traced particle, which is a solution of the Cauchy problem for the generalized quantum Fokker – Planck type kinetic equation (2.4), (2.5), and a sequence of functionals from such an operator (2.3).

References

1. V.I. Gerasimenko, The generalized Fokker-Planck kinetic equation of open quantum systems, Reports of NAS of Ukraine **1**, 3-9 (2018). doi:10.15407/dopovidi2018.01.003.

2. V.I. Gerasimenko, I.V. Gapyak, The Fokker-Planck equation with initial correlations in collisional kinetic theory, Bukovina Math. J. **3**, 52-58 (2015).

3. V.I. Gerasimenko, I.V. Gapyak, The non-Markovian Fokker-Planck kinetic equation for a system of hard spheres, Reports of NAS of Ukraine **12**, 29-35 (2014). doi:10.15407/dopovidi2014.12.029.

Dynamics of quantum correlations and kinetic equations

Viktor Gerasimenko

Institute of mathematics of the NAS of Ukraïne, Kyïv, Ukraïne

The talk provides an overview of some advances in the mathematical understanding of the nature of the kinetic equations of quantum systems of many particles. The fundamental equations of modern mathematical physics are studied, in particular, the hierarchies of evolution equations of quantum systems and their asymptotic behavior described by kinetic nonlinear equations [1].

Firstly, we discuss an approach to describing the correlations in a system of many quantum particles based on the hierarchy of evolution equations for the sequence of correlation operators, which are cumulants of the density operators (the von Neumann hierarchy). It is proved that the constructed dynamics of correlations underlies the description of the dynamics of both finitely and infinitely many quantum particles, governed by the BBGKY hierarchies for reduced (marginal) density operators or reduced correlation operators [2].

The structure of expansions by which are represented non-perturbative solutions of the Cauchy problem to these hierarchies of evolution equations of quantum systems is formulated. It is established that the concept of cumulants of the groups of operators of the von Neumann equations underlies non-perturbative expansions of solutions to hierarchies of fundamental equations that describe the evolution of observables and of the state of many quantum particles, as well as it forms the basis of the kinetic description of its collective behavior [3].

In the talk, we also consider a new approach to the problem of a rigorous description of kinetic evolution by means of reduced (marginal) observables governed by the dual BBGKY hierarchy. One of the advantages of the developed approach to the derivation of kinetic equations from underlying dynamics of many particles consists of an opportunity to construct kinetic equations with initial correlations, in particular, correlations characterizing the condensed states of a system, and to describe the processes of the propagation of initial correlations in suitable scaling limits. For this purpose, some results obtained for collisional dynamics [4,5] were generalized for quantum many-particle systems.

Firstly, we answer the following question: "What does kinetic evolution mean in terms of the evolution of observables of quantum systems?"

In what follows, we will use the notation accepted in the work [1].

If at the initial moment an observable is determined by the sequence of reduced observables $B(0) = (B_0, B_1^0(1), \ldots, B_s^0(1, \ldots, s), \ldots) \in \mathfrak{L}(\mathscr{F}_{\mathscr{H}})$, then for arbitrary $t \in \mathbb{R}$ the sequence $B(t) = (B_0, B_1(t, 1), \ldots, B_s(t, 1, \ldots, s), \ldots)$ of reduced (marginal) observables satisfies the Cauchy prob-

lem of the quantum dual BBGKY hierarchy:

$$\frac{\partial}{\partial t}B_s(t,1,\ldots,s) = \Big(\sum_{j=1}^{s}\mathscr{N}(j) + \varepsilon\sum_{j_1<j_2=1}^{s}\mathscr{N}_{\mathrm{int}}(j_1,j_2)\Big)B_s(t,1,\ldots,s) + \tag{3.1}$$

$$+\varepsilon\sum_{j_1\neq j_2=1}^{s}\mathscr{N}_{\mathrm{int}}(j_1,j_2)B_{s-1}(t,1,\ldots,j_1-1,j_1+1,\ldots,s),$$

$$B_s(t,1,\ldots,s)_{|t=0} = B_s^0(1,\ldots,s), \quad s\geq 1, \tag{3.2}$$

where the generator $\mathscr{N} = \oplus_{n=0}^{\infty}\mathscr{N}_n$ of the Heisenberg equation of n particles is defined by the formula

$$\mathscr{N}_n g_n \doteq -i(g_n H_n - H_n g_n), \tag{3.3}$$

and the self-adjoint operator $H_n = \sum_{j=1}^{n}K(j) + \varepsilon\sum_{j_1<j_2=1}^{n}\Phi(j_1,j_2)$ is the Hamilton operator of a system of n particles, that is, the operator $K(j)$ is the kinetic energy operator of j particle, Φ is the bounded operator of the pair interaction potential, $\varepsilon > 0$ is the mean field scaling parameter, and here were used units where $h = 2\pi\hbar = 1$ is a Planck constant, $m = 1$ is particle mass.

The solution of the Cauchy problem (3.1),(3.2) is represented by the following expansions:

$$B_s(t,1,\ldots,s) = \sum_{n=0}^{s}\frac{1}{n!}\sum_{j_1\neq\ldots\neq j_n=1}^{s}\mathfrak{A}_{1+n}\big(t,\{(1,\ldots,s)\setminus(j_1,\ldots,j_n)\}, \tag{3.4}$$

$$(j_1,\ldots,j_n)\big)B_{s-n}^0(1,\ldots,j_1-1,j_1+1,\ldots,j_n-1,j_n+1,\ldots,s), \quad s\geq 1,$$

where the generating operator of this expansion is the $(1+n)$-th order cumulant of the groups of operators $\mathscr{G}_n(t,1,\ldots,n)$, $n\geq 1$, of the n-particle Heisenberg equation:

$$\mathfrak{A}_{1+n}(t,\{(1,\ldots,s)\setminus(j_1,\ldots,j_n)\},(j_1,\ldots,j_n)) \doteq$$
$$\sum_{\mathrm{P}:(\{(1,\ldots,s)\setminus(j_1,\ldots,j_n)\},(j_1,\ldots,j_n))=\cup_i X_i}(-1)^{|\mathrm{P}|-1}(|\mathrm{P}|-1)!\prod_{X_i\subset\mathrm{P}}\mathscr{G}_{|\theta(X_i)|}(t,\theta(X_i)), \quad n\geq 0,$$

and used notation accepted in the work [1].

Note that traditionally, the evolution of quantum many-particle systems is described within the framework of the evolution of the state governed by the BBGKY hierarchy for reduced (marginal) density operators [3].

To give an answer to the above-formulated question, we consider the scaling asymptotic behavior of a solution of the Cauchy problem (3.4) for the dual BBGKY hierarchy (3.1), (3.2) in the case of the mean-field limit, or, in other words, we consider the foundations of the description of the kinetic evolution of systems of many quantum particles within the framework of observables.

Note that one of the advantages of such an approach to the description of kinetic evolution is the possibility of describing the propagation of initial correlations in scaling limits. In other words, such an approach to the derivation of kinetic equations allows us to formulate kinetic equations in the case of more general initial states, which describe not only the gases of quantum particles but also systems in condensed states.

Suppose that at the initial moment of time there exists the mean-field limit of reduced observables (3.2) in the sense of $*$-weak convergence of the space of bounded operators $\mathfrak{L}(\mathscr{H}_s)$

$$\mathrm{w}^* - \lim_{\varepsilon \to 0} \left(\varepsilon^{-s} B_s^{\varepsilon,0} - b_s^0 \right) = 0, \tag{3.5}$$

where $\varepsilon > 0$ is a scaling parameter.

Then the following limit theorem holds for reduced observables (3.4), which are the solution of the dual BBGKY hierarchy (3.1).

If the condition (3.5) is satisfied, then for an arbitrary finite time interval there is a mean-field limit for the sequence of reduced observables (3.4) in the same sense

$$\mathrm{w}^* - \lim_{\varepsilon \to 0} \left(\varepsilon^{-s} B_s(t) - b_s(t) \right) = 0, \tag{3.6}$$

where the reduced observables $b_s(t)$, $s \geq 1$, are determined by the following expansions:

$$b_s(t,1,\ldots,s) = \sum_{n=0}^{s-1} \int_0^t dt_1 \ldots \int_0^{t_{n-1}} dt_n \, \mathscr{G}_s^0(t-t_1) \sum_{i_1 \neq j_1 = 1}^s \mathscr{N}_{\mathrm{int}}(i_1,j_1) \mathscr{G}_{s-1}^0(t_1-t_2) \ldots \tag{3.7}$$

$$\mathscr{G}_{s-n+1}^0(t_{n-1}-t_n) \sum_{\substack{i_n \neq j_n = 1, \\ i_n, j_n \neq (j_1,\ldots,j_{n-1})}} \mathscr{N}_{\mathrm{int}}(i_n,j_n) \mathscr{G}_{s-n}^0(t_n) b_{s-n}^0((1,\ldots,s) \setminus (j_1,\ldots,j_n)), \quad s \geq 1,$$

and for the group of operators of non-interacting particles, the notation was used

$$\mathscr{G}_{s-n+1}^0(t_{n-1}-t_n) \equiv \prod_{j \in (1,\ldots,s) \setminus (j_1,\ldots,j_{n-1})} \mathscr{G}_1(t_{n-1}-t_n,j).$$

Thus, in the mean-field limit, the collective behavior (kinetic evolution) of quantum systems of many particles is described in terms of the sequence of limiting reduced observables (3.7) whose evolution is governed by the Cauchy problem of the dual Vlasov hierarchy (3.8),(3.9):

$$\frac{\partial}{\partial t} b_s(t,1,\ldots,s) = \sum_{j=1}^s \mathscr{N}(j) b_s(t,1,\ldots,s) + \sum_{j_1 \neq j_2 = 1}^s \mathscr{N}_{\mathrm{int}}(j_1,j_2) b_{s-1}(t,(1,\ldots,s) \setminus (j_1)), \tag{3.8}$$

$$b_s(t,1,\ldots,s) \big|_{t=0} = b_s^0(1,\ldots,s), \quad s \geq 1. \tag{3.9}$$

Now we consider the relationship of collective behavior within the mean-field approximation described by the dual Vlasov hierarchy (3.8) for the limiting observables and by the Vlasov kinetic equation for the state of a typical particle in a system of many quantum particles. Let the initial state of a quantum system of many particles be determined by a one-particle density operator and correlation operators (Maxwell–Boltzmann statistics)

$$f^{(cc)} = \left(I, f_1^0(1), g_2^0(1,2) \prod_{i=1}^2 f_1^0(i), \ldots, g_n^0(1,\ldots,n) \prod_{i=1}^n f_1^0(i), \ldots \right), \tag{3.10}$$

where the correlations of the initial states of the particles are determined by the operators $g_n^0 \in \mathfrak{L}_0^1(\mathscr{H}_n), n \geq 2$. We emphasize that this assumption (3.10) with respect to the initial state is typical for the kinetic description of systems of many particles in condensed states, which are characterized by correlations.

Applying the method of derivation of kinetic equations based on the hierarchy of kinetic equations for the observables [5], for an arbitrary finite time interval, we establish that the state is described by the sequence $f(t) = (I, f_1(t), \ldots, f_n(t, 1, \ldots, n), \ldots)$ of limiting reduced density operators where a one-particle density operator is governed by the quantum Vlasov kinetic equation with initial correlations

$$\frac{\partial}{\partial t} f_1(t, 1) = \mathscr{N}^*(1) f_1(t, 1) + \tag{3.11}$$

$$\mathrm{Tr}_2 \mathscr{N}_{\mathrm{int}}^*(1, 2) \prod_{i_1=1}^{2} \mathscr{G}_1^*(t, i_1) g_2^0(1, 2) \prod_{i_2=1}^{2} (\mathscr{G}_1^*)^{-1}(t, i_2) f_1(t, 1) f_1(t, 2),$$

and the limiting density operators $f_k(t, 1, \ldots, k), k \geq 2$, are determined by the following expressions:

$$f_k(t, 1, \ldots, k) = \prod_{i_1=1}^{k} \mathscr{G}_1^*(t, i_1) g_k^0(1, \ldots, k) \prod_{i_2=1}^{k} (\mathscr{G}_1^*)^{-1}(t, i_2) \prod_{j=1}^{k} f_1(t, j), \quad k \geq 2, \tag{3.12}$$

where the inverse group of operators to group is denoted by $(\mathscr{G}_1^*)^{-1}(t)$.

We note that the kinetic equation (3.11) is a non-Markov kinetic equation. For pure states, equation (3.11) reduces to the Hartree kinetic equation with initial correlations. For the initial states of the system of statistically independent particles, the kinetic equation (3.11) coincides with the quantum Vlasov equation, and reduced (marginal) density operators (3.12) describe the process of propagation of the initial chaos.

Thus, the alternative method of describing the evolution of states of quantum systems of many particles in the mean-field approximation is based on the non-Markovian Vlasov kinetic equation with initial correlations (3.11). The above results can be extended to systems of many bosons or fermions.

To describe the evolution of the states of quantum many-particle systems, there is an alternative approach that is based on the dynamics of correlations [4]. In this approach, a state of finitely many quantum particles is described with the employment of operators determined by the cluster expansions of the density operators that are governed by the so-called von Neumann hierarchy. It was established that the constructed dynamics of correlation underlie the description of the dynamics of infinitely many quantum particles governed by the BBGKY hierarchy for marginal density operators or the hierarchy of nonlinear evolution equations for marginal correlation operators, i.e., of the cumulants of marginal density operators [3]. We emphasize the importance of the mathematical description of the processes of the creation and propagation of correlations in quantum systems, in particular, for numerous applications.

The purpose of this talk was to analyze the development and current advances of the theory of evolution equations for systems of many quantum particles, in particular, quantum kinetic equations and their relations to the fundamental equations that describe the laws of nature.

References

1. V.I. Gerasimenko, Kinetic equations and hierarchies of evolution equations of quantum systems, Preprint arXiv:2107.10872, (2021). https://doi.org/10.48550/arXiv.2107.10872

2. V.I. Gerasimenko, Processes of creation and propagation of correlations in large quantum particle system, Panorama of Contemporary Quantum Mechanics – Concepts and Applications. London: InTech, 2019, 31–47. https://doi.org/10.5772/intechopen.82836

3. V.I. Gerasimenko, Hierarchies of quantum evolution equations and dynamics of many-particle correlations, Statistical Mechanics and Random Walks: Principles, Processes and Applications, N.Y.: Nova Sci. Publ., Inc., 2013, 233–288.

4. V.I. Gerasimenko, I.V. Gapyak, Propagation of correlations in a hard-sphere system. J. Stat. Phys. **189**, 2 (2022). https://doi.org/10.1007/s10955-022-02958-8

5. V.I. Gerasimenko, I.V. Gapyak, Advances in theory of evolution equations of many colliding particles, Modern Problems of Mathematics and its Applications. Kyïv: IM, 729–804, 2023. https://doi.org/10.3842/trim.v20n1.528

Quantum algorithms for detection of the energy levels of spin systems and graph properties with quantum programming

Kh. P. Gnatenko[1], H. P. Laba[2], V. M. Tkachuk[1]

[1] Professor Ivan Vakarchuk Department for Theoretical Physics, Ivan Franko National University of Lviv, 12, Drahomanov St., Lviv, 79005, Ukraine
[2] Department of Applied Physics and Nanomaterials Science, Lviv Polytechnic National University, 5 Ustiyanovych St., 79013 Lviv, Ukraine

We propose quantum algorithms for the detection of the energy levels of spin systems on a quantum computer. We show that the time dependence of the mean value of a physical quantity is related to the energies of a quantum system in the case when the operator of the physical quantity anticommutes with the Hamiltonian of the system [1]. Namely for the mean value of physical quantity represented by operator $\hat{A}$ the following relation is satisfied

$$A(t) = \langle \psi(t)|\hat{A}|\psi(t)\rangle = \sum_{i,j} c_i c_j^* A_{ij} e^{i2E_j t/\hbar}, \tag{4.1}$$

where $|\psi(t)\rangle = e^{-iHt/\hbar}|\psi_0\rangle$, H is the Hamiltonian of a system, $|\psi_0\rangle$ is an initial state, $A_{ij} = \langle E_i|\hat{A}|E_j\rangle$ is matrix element of operator $\hat{A}$, $|E_i\rangle$ are eigenstates of the Hamiltonian, c_i are coefficients of expansion of initial state $|\psi_0\rangle$ over the eigenstates of the Hamiltonian $|\psi_0\rangle = \sum_i c_i|E_i\rangle$. Therefore, studying the evolution of the mean value of the operator with quantum programming gives the possibility to determine the energy levels. On the basis of the proposed algorithm energy levels of spin systems, namely spin in a magnetic field, spin chain, Ising model on the squared lattice are detected on IBM's quantum computers [1,2].

In the case when for a given Hamiltonian the anticommuting operator does not exist, we propose a quantum algorithm based on studies of the evolution of only one probe spin. For this purpose we propose to construct the total Hamiltonian in the following form

$$H_T = \sigma_0^z(H + C), \tag{4.2}$$

where H is the Hamiltonian of the system, C is a constant added to shift the energy levels of H to the positive ones, σ_0^z is the Pauli matrix of additional spin (ancilla qubit). Note, that it is easy to find operators that anticommute with the Hamiltonian H_T. They are σ_0^x, σ_0^y. So, on the basis of studies of the time dependence of the mean value of σ_0^x or σ_0^y, we can detect the energy levels of the total Hamiltonian H_T and therefore the energy levels of the system. The algorithm was applied for studies of the energy levels of the spin chain in a magnetic field, triangle spin cluster, and Ising model on a squared lattice in the magnetic field on IBM's quantum device. The results of quantum calculations are in agreement with the theoretical ones [3].

It is worth noting that the proposed quantum protocols are efficient for the estimation of the energy levels of many-spin systems. The methods open the possibility of achieving quantum supremacy with the development of multi-qubit quantum computers.

On the basis of the proposed algorithms, we observe spin-1 tunneling on IBM's quantum computer [4]. We realize spin-1 with two spins-1/2. We detect the splitting of the energy levels as a result of tunneling on IBM's quantum device ibmq-bogota with studying of the evolution of probe spin.

Also, a quantum algorithm for the detection of the graph properties, namely the number of edges, triangles, and squares in a graph is developed [5]. We consider graph states as follows

$$|\psi\rangle = e^{-\frac{it}{2\hbar}\sum_{i,j}J_{ij}\sigma_i^x\sigma_j^x}|00...0\rangle. \tag{4.3}$$

The states can be represented by graphs with vertices corresponding to spins and edges representing interactions between them, J_{ij} are interaction coupling constants related to the elements of adjacency matrix A_{ij}. We obtain that the geometric properties of evolutionary graph states of spin systems with Ising Hamiltonian are related to the graph properties. Namely, we found that such geometric characteristics as the velocity of quantum evolution, the curvature, and the torsion of the states are related to the total number of edges, triangles, and squares. The relations read

$$v = \frac{\gamma J}{\hbar}\sqrt{k_2}, \tag{4.4}$$

$$\bar{\kappa} = \frac{1}{k_2^2}\left(k_2 + 3k_2(k_2-1) + 4!k_4\right)^2 - 1, \tag{4.5}$$

$$\bar{\tau} = \bar{\kappa} - \frac{6^2k_3^2}{k_2^3}, \tag{4.6}$$

where v is the velocity of quantum evolution, $\bar{\kappa}$ is the curvature and $\bar{\tau}$ is the torsion, constants k_2, k_3, k_4 are the total number of edges, triangles and squares in the graph. The studies are based on the relations of the geometric properties of evolutionary graph states with fluctuations of energy obtained in [6].

Graph states corresponding to a chain, a triangle, and a square are studied. We apply the algorithm to detect the number of edges, triangles, and squares in the corresponding graphs on IBM's quantum computer ibmq-manila [5]. The developed quantum algorithm gives a possibility to achieve quantum supremacy in finding the number of edges, triangles, and squares in graphs with complicated structures with the development of quantum devices.

We also study the geometric measure of entanglement of quantum graph states [7,8]. It is defined as a minimal squared Fubini-Study distance between the entangled state $|\psi\rangle$ and a set of non-entangled states $|\psi_s\rangle$,

$$E(|\psi\rangle) = \min_{|\psi_s\rangle}(1 - |\langle\psi|\psi_s\rangle|^2), \tag{4.7}$$

see [9]. In paper [10] it was obtained that the geometric measure of entanglement of a spin with a quantum system in the state $|\psi\rangle = a|0\rangle|\Phi_1\rangle + b|1\rangle|\Phi_2\rangle$, (here a, b are constants, $|\Phi_1\rangle$, $|\Phi_2\rangle$ are states of quantum system $\langle\Phi_i | \Phi_i\rangle = 1$, $i = 1,2$) is related to its mean value. The relation has the following form

$$E(|\psi\rangle) = \frac{1}{2}(1 - |\langle\boldsymbol{\sigma}\rangle|), \tag{4.8}$$

where $|\langle\boldsymbol{\sigma}\rangle| = \sqrt{\langle\boldsymbol{\sigma}\rangle}$. On the basis of the relation, we find analytically the geometric measure of entanglement of a spin with other spins for graph states corresponding to the arbitrary graph structure. We consider graph states prepared with the action of the operator of the evolution of the Ising model (4.3). Also, graph states prepared with the action of the controlled phase shift operator are studied.

$$|\psi_G(\phi,\alpha,\theta)\rangle = \prod_{(i,j)\in E} CP_{ij}(\phi)\,|\psi(\alpha,\theta)\rangle^{\otimes V}, \qquad (4.9)$$

$$|\psi(\alpha,\theta)\rangle = \cos\frac{\theta}{2}\,|0\rangle + e^{i\alpha}\sin\frac{\theta}{2}\,|1\rangle, \qquad (4.10)$$

here $CP_{ij}(\phi)$ is the controlled phase shift gate that acts on the qubits $q[i]$, $q[j]$. The states are associated with graph $G(V,T)$.

It is obtained that the geometric measure of entanglement of a spin is related to the degree of vertex which represents it in the graph. In the case of quantum graph states (4.3) we find that the entanglement of a spin labeled by index l reads

$$E_l = \frac{1}{2} - \frac{1}{2}|\cos^{n_l}\phi|, \qquad (4.11)$$

where $\phi = 2Jt/\hbar$, n_l is the degree of vertex which represents spin l in the graph. In the case of state $|\psi_G(\phi,\alpha,\theta)\rangle$ the entanglement of qubit $q[l]$ with other qubits is given by

$$E_l = \frac{1}{2} - \frac{1}{2}\sqrt{\sin^2\theta\left(\cos^2\frac{\phi}{2} + \sin^2\frac{\phi}{2}\cos^2\theta\right)^{n_l} + \cos^2\theta}, \qquad (4.12)$$

where n_l is the degree of vertex which represents qubit $q[l]$. The geometric measure of entanglement of the graph states is calculated on IBM's quantum computers [7,8]. The results of quantum calculations are in good agreement with the theoretical ones.

References

1. Gnatenko Kh. P., Laba H. P., Tkachuk V. M. Energy levels estimation on a quantum computer by evolution of a physical quantity. Phys. Lett. A. **424**, 127843 (2022).

2. IBM Q experience. https://quantum-computing.ibm.com/

3. Gnatenko Kh. P., Laba H. P., Tkachuk V. M. Detection of energy levels of a spin system on a quantum computer by probe spin evolution. Eur. Phys. J. Plus **137**, 522 (2022).

4. Gnatenko Kh. P., Tkachuk V. M. Observation of spin-1 tunneling on a quantum computer. Eur. Phys. J. Plus. 138, 346 (2023).

5. Gnatenko Kh. P., Laba H. P., Tkachuk V. M. Geometric properties of evolutionary graph states and their detection on a quantum computer. Phys. Lett. A. **452**, 128434 (2022).

6. Laba H. P., Tkachuk V. M. Geometric characteristics of quantum evolution: curvature and torsion. Condens. Matter Phys. **20**, 13003 (2017).

7. Gnatenko Kh. P., Tkachuk V. M. Entanglement of graph states of spin system with Ising interaction and its quantifying on IBM's quantum computer. Phys. Lett. A. **396**, 127248 (2021).

8. Gnatenko Kh. P., Susulovska N. A. Geometric measure of entanglement of multi-qubit graph states and its detection on a quantum computer. EPL (Europhys. Lett.) **136**, 40003 (2021).

9. Shimony A. Degree of entanglement. Ann. N.Y. Acad. Sci. **755**, 675 (1995).

10. Frydryszak A. M., Samar M. I., Tkachuk V. M. Quantifying geometric measure of entanglement by mean value of spin and spin correlations with application to physical systems. Eur. Phys. J. D **71**, 233 (2017).

Quantal and semiclassical study of the elastic scattering and charge transfer in cold H+H$^+$ collisions

Mykhaylo Khoma

Institute of Electron Physics, NASU, Uzhhorod, Ukraine

The study of the elementary processes occurring at proton impact on atomic hydrogen is important for many applications such as astrophysical and fusion plasma. In the present study, we compute the cross sections of the elastic scattering (EL)

$$H(1s) + H^+ \rightarrow H(1s) + H^+ \tag{5.1}$$

and the resonant charge transfer (CT)

$$H(1s) + H^+ \rightarrow H^+ + H(1s), \tag{5.2}$$

at proton collision with atomic hydrogen for the energy range of $10^{-10} \leq E_{\mathrm{c.m.}} \leq 10$ eV. Here $E_{\mathrm{c.m.}}$ is the collision energy in the center-of-mass frame. Reactions (5.1) and (5.2) have been the subject of active study for many decades [1-4].

For the energy range considered here, only the two lowest electronic states of H$_2{}^+$, the $1s\sigma_g$ *gerade* (g) and $2p\sigma_u$ *ungerade* (u), are involved. Thus, the cross sections for reactions (5.1) and (5.2) may be obtained from solutions of uncoupled single-channel Schrödinger equations of the form

$$\left(\frac{\mathrm{d}^2}{\mathrm{d}R^2} + k^2 - 2\mu V_{g,u}^{(l)}(R) \right) \psi_{g,u}^{(l)}(R) = 0, \tag{5.3}$$

where $k^2 = 2\mu E_{\mathrm{c.m.}}$, μ is the system reduced mass, l is the orbital angular momentum of the collision system, $V_{g,u}^{(l)}(R)$ is the adiabatic potential for either the $1s\sigma_g$ or $2p\sigma_u$ state, and $\psi_{g,u}^{(l)}(R)$ is the radial wave function for the corresponding reaction channel. The adiabatic potential $V_{g,u}^{(l)}(R)$ reads

$$V_{g,u}^{(l)}(R) = E_{g,u}^{\mathrm{BO}}(R) + \frac{l(l+1)}{2\mu R^2}, \tag{5.4}$$

where $E_{g,u}^{\mathrm{BO}}(R)$ is the Born-Oppenheimer energy of the corresponding reaction channel. We compute the $E_{g,u}^{\mathrm{BO}}(R)$ energy as the solution to the two-Coulomb-center problem eZ_1Z_2 by the method of the continued fractions.

The integral cross sections are determined from the scattering phase shifts. Due to the quantum indistinguishability of identical particles (as in the present case), the two different sets of elastic scattering cross sections, ELi (for indistinguishable) and ELd (for distinguishable) particles approach are produced. Both the fully quantal and the semiclassical (JWKB) approaches were utilized in the present calculations. Our computed cross sections (in a.u., $a_0^2 = 2.8003 \times 10^{-17} \mathrm{cm}^2$) are compared with the results of other authors and presented in Tab. 1 and Fig. 1.

Table 5.1: The integral cross section (in a_0^2) for charge transfer. The present fully quantal and JWKB calculations.

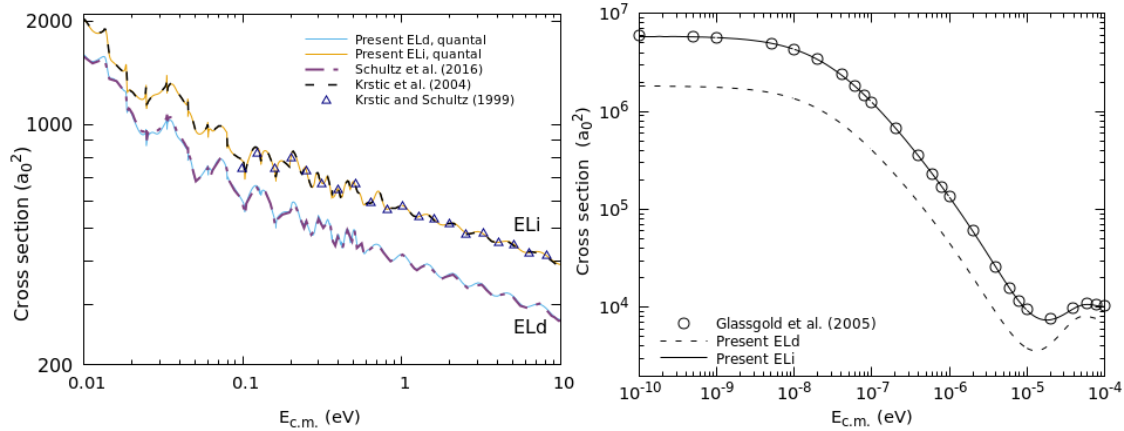| $E_{c.m.}$ (eV)	Present, quantal	Present, JWKB
0.1254	205.247	195.32
0.3	184.318	187.99
0.5100	166.518	165.99
1.0	162.251	162.16

Figure 5.1: (left panel) Elastic distinguishable (ELd) and elastic indistinguishable (ELi) integral cross sections for center-of-mass collision energies within the range of 0.01–10 eV. Solid lines, the present quantal calculations; $--$, the quantal calculations of Schultz *et al.* [1]; $-\cdot-$, the quantal calculations of [2]; $\triangle$, the JWKB calculations of [3]; (right panel) Integral elastic cross sections for the energy range of 10^{-10}–10^{-4} eV. Lines, the present calculations of $\sigma_{EL}^{(d)}$ and $\sigma_{EL}^{(i)}$; $\bigcirc$, the $\sigma_{EL}^{(i)}$ calculations of [4].

References

1. Schultz D. R., Ovchinnikov S. Yu., Stancil P. C., Zaman T. Elastic, charge transfer, and related transport cross sections for proton impact of atomic hydrogen for astrophysical and laboratory plasma modeling. J. Phys. B. **49**, 084004 (2016). https://doi.org/10.1088/0953-4075/49/8/084004

2. Krstić P. S., Macek J. H., Ovchinnikov S. Yu., Schultz D. R. Analysis of structures in the cross sections for elastic scattering and spin exchange in low-energy $H^+ + H$ collisions. Phys. Rev. A **70**, 042711 (2004). https://doi.org/10.1103/PhysRevA.70.042711

3. Krstić P. S., Schultz D. R. Elastic scattering and charge transfer in slow collisions: isotopes of H and H^+ colliding with isotopes of H and with He. J. Phys. B. **32**, 3485-3509 (1999). https://doi.org/10.1088/0953-4075/32/14/317

4. Glassgold A. E., Krstic P. S., Schultz D. R. $H^+ + H$ scattering and ambipolar diffusion heating. Astrophys. J. **621**, 808-816 (2005). https://doi.org/10.1086/427686

Azobenzene-Based Polymer as a Photoactive Material: Simulation, Preparation and Properties

I. Tkachenko[1,2], <u>Yu. Kurioz</u>[1], K. Akunuri[3], R. Kravchuk[1], A. Glushchenko[4], V. Shevchenko[2], T. Vo[3], V. Nazarenko[1]

[1]Institute of Physics, Kiev 03039, Ukraine
[2]Institute of Macromolecular Chemistry of the NAS of Ukraine, Kharkivske Shosse 48, 02160, Kyiv, Ukraine
[3]Johns Hopkins University, Whiting School of Engineering, 3400 North Charles Street, Baltimore, MD 21218, USA
[4] Department of Physics, University of Colorado at Colorado Springs, 1420 Austin Bluffs Parkway, Colorado Springs, CO 80918, USA

Light-responsive polymers show great promise in various applications, such as reconfigurable photonic elements and optical-to-mechanical energy conversion. Azobenzene chromophores are popular for their reversible conformational changes (trans-cis-trans photoisomerization) absorption of UV or visible light. An intriguing aspect of light-responsive polymers is their capacity to exhibit anisotropic behavior under polarized light irradiation. Thus, during azobenzene's trans-cis-trans isomerization within the polymer, the orientation of the units shifts, becoming perpendicular to the incident light polarization. This induces a conformational change in the macromolecules, resulting in photoinduced alignment of the azobenzene fragments. As a consequence, the polymer film exhibits birefringence upon illumination. This phenomenon is particularly relevant for the design of polarization holographic gratings and the efficient control of photoalignment. In this context, polymers with azobenzene side chains are widely used, while polymers with azobenzene moieties in the backbone face problems due to limited solubility, mechanical properties and film forming ability. Overcoming these challenges is essential to unlock the full potential of light-responsive polymers with azobenzene functionalization in the main chain.

In this study, we synthesized and characterized a polymer that combines azobenzene and octafluorobiphenylene (OFB) units alongside with meta-linked fragments in the backbone. The resulting polymer is azo-containing fluorinated poly(arylene ether) (Azo-FPAE). The incorporation of OFB units improves solubility (due to the lipophilicity of fluorine atoms), enhances chemical and thermal stability, and influences molecular packing due to the nonplanarity of OFB's aromatic rings. Furthermore, according to the literature, the incorporation of fluorinated units is known to improve the optical and electro-optical properties of the polymer, leading to a lower refractive index, reduced optical losses, and enhanced hyperpolarization. We also incorporated meta-phenoxy units based on our previous research, which demonstrated improved solubility, thermostability, and mechanical properties in such meta-connected polymers.

The Azo-FPAE was synthesized by the aromatic nucleophilic substitution reaction from decafluorobiphenyl 1 (DFB) and hydroxyl-substituted azo-based monomer 2 (4,4'-{(2,2',3,3', 5,5',6,6'-octafluorobiphenyl-4,4'-diyl)bis[oxy-3,1-phenylenediazene-2,1-diyl]}diphenol) in dimethylacetamide (DMAc) in the presence of excess potassium carbonate as a base.
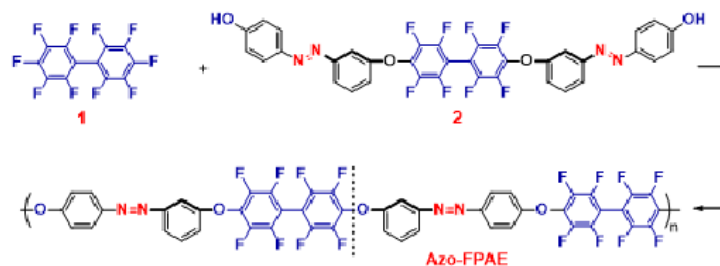
We introduced an azo group into the structure of polymer through the OH-based component, namely V-type monomer 2 (conjugation system D-π-A-π-D), in which the electron acceptor component (A) is situated between the two donor (D) units. Remarkably, monomer 2 can be regarded as an a-b-a trimer, comprising a DFB residue (b) and a para/meta-substituted azo-diphenol residue (a). Consequently, the polymer structure can be simplified as the result of the interaction between DFB (**b** in **a-b-a** trimer) and 3-((4-hydroxyphenyl)diazenyl)phenol (**a** in **a-b-a** trimer). Nevertheless, in our perspective, monomer 2 was obtained more easily through a straightforward diazotization reaction of the corresponding fluorinated meta-linked aromatic diamine followed by azo coupling with phenol.

The Azo-FPAE polymer, obtained as an orange fibrous solid, exhibited complete solubility in chloroform and DMAc, while it was insoluble in alcohols. This solubility behavior allows for the casting of the copolymer from solution, yielding high-quality self-supporting films that are mechanically strong and easy to handle. The success of the synthesis of the Azo-coFPAE was confirmed with ^{1}H NMR, ^{19}F NMR, FTIR and Raman spectroscopy techniques. The electronic absorption spectrum of the prepared azobenzene-modified polymer in DMAc solution exhibit two characteristic absorption bands. The high intensity band at around 336 nm is related to π-π* transition of the trans form of the azobenzene moiety. The weak band at $\sim$440 nm originates from typical n-π* transition.

Thermal properties of the resulting Azo-FPAE were investigated by differential scanning calorimetry (DSC) and thermal gravimetric analysis (TGA). Owing to the high content of fluorinated units, the polymer had good thermal stability and exhibited a one-step pattern of decomposition. It demonstrated a temperature of 405°C at 5% weight loss (T$_{5\%}$), indicating its suitability for various applications. DSC measurements revealed the amorphous nature of the copolymer because no melting endotherm peak was found from the first and second heating DSC scans. Note, two glass transition temperatures (T$_g$) are revealed for Azo-FPAE: T$_{g1}$ is about 151 ^{o}C and T$_{g2}$ is about 184 ^{o}C. This indicates that the polymer structure consists of two different amorphous regions.

Generally, various interactions can occur within the polymer, including H- and J-aggregation of azobenzene fragments, π_{Ar}-π_{ArF} (fluorine) stacking interactions between non-fluorinated aromatic units and perfluoroaromatic fragments, and other weak interactions. The nonplanarity of the OFB fragment rings is caused by the covalent bonds between perfluorinated phenylene fragments, which leads to the contortion of polymer chains. All these factors influence the packing of polymer chains and the available free volume within the polymer, which are crucial for processes such as photoisomerization and photoorientation.

To address these questions and gain further insights into the chain conformations and interactions, we first develop a coarse-grained computational model aimed at preserving the relevant geometry

of the Azo-FPAE monomer for use in molecular dynamics simulations. Specifically, our model directly incorporates the shape of each subunit of the monomer as opposed to conventional spherical-bead approximations. This approach enables us to preserve the relevant stacking of the aromatic units using a minimal model that can capture hierarchical, mesoscale organization – particularly relevant for subsequent property characterization. As such, results from both theoretical and experimental studies combine to provide comprehensive understanding of the azo-based system.

Quantum Anomalies have Classical Origin

Robert R. Lompay

Uzhhorod National University, Uzhhorod, Ukraine

Quantum anomalies (ie, the violation of the conservative nature of the classical Noether currents by quantum radiative corrections, for a review see [1]) are one of the most intriguing and mysterious phenomena of quantum field theory. It is commonly believed that they have a purely quantum origin (they are an artifact of the renormalization procedure) and therefore, they in principle cannot be derived within the framework of the classical theory. The purpose of the current research is to demonstrate that the anomalies can arise naturally in the classical theory of spatially bounded field systems. Exploring as an example the classical electrodynamics of massless fermions in the space-time domain Ω of a finite size, we show that the famous Adler-Bell-Jackiw (ABJ) anomaly $\partial_\nu j_{5vac}^\nu = cF_{\mu\nu}{}^*F^{\mu\nu}$ is a simple consequence of the requirements of the spatial boundedness of the field system under consideration (ie non-spreading of the fields beyond the region Ω) and the gauge invariance. The main stages of our research are as follows.

We consider first the theory of the free massless Dirac field ψ in the region Ω ($\partial\Omega = \Sigma_1 \cup \Sigma_2 \cup B_{12}$, where Σ_1, Σ_2 are spacelike, and B_{12} is timelike). We require that during the evolution the field must remain localized in Ω, and the Dirac equation is fulfilled everywhere in $\overline{\Omega} = \Omega \cup B_{12}$ (that is, both in the bulk Ω, and *on its boundary B_{12}*). These requirements can be satisfied only if we introduce a *surface (i.e localized on B_{12}) fermion source ζ*. It is shown that the including of its in the Lagrangian makes the variational problem well-posed, and the variational principle allows us to obtain the Dirac equation $i\gamma^\mu \partial_\mu \psi = 0$ (the equation of motion in the bulk Ω), as well as *the junction conditions $\psi|_{B_{12}} = \mu\zeta$* (the equation of motion on the boundary B_{12}). The last relation will be chirally invariant if ζ has the same transformation properties as ψ.

We consider then the electromagnetic field $F^{\mu\nu}$ interacting with an external electric current j^ν. The requirements of the localization of the field in Ω (both its electric $\vec{E}$ and magnetic $\vec{H}$ components) and fulfillment of the Maxwell equations in $\overline{\Omega}$ forces us to introduce *surface electric i^ν and magnetic $'i^\nu$ currents*. It is shown that they can be combined into a unique tensor $i^{\mu\nu}$ ($i^\nu = i^{\perp\nu}$, $'i^\nu = {}^*i^{\perp\nu}$), so the surface sources are of the dipole type (here $\perp$ means the component orthogonal to B_{12}, and $*$ is the Hodge star). The standard Maxwell action functional allows us to derive junction conditions for $F^{\perp\nu}$ components only. We overcome this difficulty by constructing a *complex* action functional whose imaginary part is the Chern-Simons form. It is shown that the inclusion of the surface currents $i^{\mu\nu}$ leads to a well-posed variational problem and allows us to obtain both, the Maxwell equation $\partial_\mu F^{\mu\nu} = -j^\nu$ and the juction conditions $F^{\mu\nu}|_{B_{12}} = i^{\mu\nu}$ *for all components* of the electromagnetic field. The resulting theory can be formulated in terms of the self-dual field $F_-^{\mu\nu} = F^{\mu\nu} - i{}^*F^{\mu\nu}$ (*the Riemann-Silberstein vector $\vec{\mathcal{E}} = \vec{E} + i\vec{H}$*) and the self-dual sources $i_-^{\mu\nu} = i^{\mu\nu} - i{}^*i^{\mu\nu}$. The analysis of the canonical structure of the theory shows that, unlike the case of an electromagnetic field in the infinite space, in our case the components of the vector $\vec{\mathcal{E}}$ are kinematically independent (ie they commute). Alternatively, but equivalently, the theory can be formulated in terms of antiself-dual quantities $F_+^{\mu\nu}$, $i_+^{\mu\nu}$. It should be noted that the Riemann-Silberstein vector $\vec{\mathcal{E}}$ plays an important role in modern studies of optical helicity (see, for example, [2] and references therein).

Finally, we consider the full dynamical theory of interacting the massless electron-positron and the electromagnetic fields localized in Ω. The fermionic surface source ζ is a charged field, and therefore it must contribute to the surface currents $i^{\mu\nu}$. The interaction of ψ and ζ with the electromagnetic field (with the potential A_μ) is fixed by the requirement of the gauge invariance of the theory in $\overline{\Omega}$. The analysis of the dynamical conservation of the total electric current J^ν (which includes both bulk j^ν and surface i^ν currents) leads to the identification $i^{\mu\nu} = e\mu\overline{\zeta}S^{\mu\nu}\zeta = e\mu\overline{\zeta}_L S^{\mu\nu}\zeta_R + e\mu\overline{\zeta}_R S^{\mu\nu}\zeta_L = i_+^{\mu\nu} + i_-^{\mu\nu}$ and to the junction conditions $F_\pm^{\mu\nu}|_{B_{12}} = i_\pm^{\mu\nu}$ (here $S^{\mu\nu}$ is the spin matrix, and ζ_R and ζ_L are the right and left spinors, respectively). Unlike the bulk current vector $j^\nu = e\overline{\psi}\gamma^\nu\psi = e\overline{\psi}_R\gamma^\nu\psi_R + e\overline{\psi}_L\gamma^\nu\psi_L = j_R^\nu + j_L^\nu$, each of $i_\pm^{\mu\nu}$ contains fields of *opposite* chirality and therefore the are not invariant under chiral transformations (γ_5-rotations). When $\psi \to \exp(i\alpha\gamma_5)\psi$, then $i_\pm^{\mu\nu} \to \exp(\pm i2\alpha)i_\pm^{\mu\nu}$. Therefore, in order to ensure the fulfillment of the junction conditions (the field equations on B_{12}!), every γ_5-rotations of fermions must be accompanied by dual rotations ($*$-rotations) of the electromagnetic field $F_\pm^{\mu\nu} \to \exp(2\alpha*)F_\pm^{\mu\nu} = \exp(\pm i2\alpha)F_\pm^{\mu\nu}$. We show that for such extended (γ_5- plus $*$-) chiral rotations, the corresponding current J_5^ν is nothing but the *total helicity current* (the sum of the helicity currents of the electron-positron J_{5EP}^ν and the electromagnetic J_{5EM}^ν fields), and that its conservation *reproduces the chiral anomaly of ABJ*, $\partial_\nu J_5^\nu = \partial_\nu J_{5EP}^\nu - cF_{\mu\nu}{}^*F^{\mu\nu} = 0$.

The validity of the proposed classical mechanism of the generation of the chiral anomaly can be verified experimentally. The predictable effect will consist in the helicity flip of a circularly polarized electron beam moving along an optical circular waveguide in which an electromagnetic field of the suitable configuration is excited (an optical instanton). The theoretical calculation of such a field, as well as a multiplicity of various other processes having place in such a system, can be performed by the methods of the Penrose twistor theory [3].

Some features, in particular symmetry properties, of the electrodynamics with dipole-type currents are also discussed. Based on them, a possible theoretical explanation of the problem (of non-existence) of the electric dipole moment of the electron is proposed.

The current investigation is a part of a broader research program of the investigation of the classical and quantum kinematics and dynamics of spatially bounded field systems. Some directions of further investigations and their perspectives are outlined.

References

1. Morozov, A., Anomalies in gauge theories, Soviet Physics - Uspekhi **29**, 993-1039 (1986). https://doi.org/10.1070/PU1986v029n11ABEH003537.

2. Bliokh, K., Bekshaev, A., Nori, F., Dual electromagnetism: helicity, spin, momentum and angular momentum, New Journal of Physics **15**, 033026 [28 pages] (2013). https://doi.org/10.1088/1367-2630/15/3/033026.

3. Penrose, R., MacCallum M., Twistor theory: an approach to the quantisation of fields and space-time, Physics Reports **6**, 241-316 (1972). https://doi.org/10.1016/0370-1573(73)90008-2.

Variational optimization of iPEPS with CTMRG on the original lattice

Illya Lukin[1,2]

[1]Karazin Kharkiv National University, Svobody Square 4, 61022 Kharkiv, Ukraine
[2]Akhiezer Institute for Theoretical Physics, NSC KIPT, Akademichna 1, 61108 Kharkiv, Ukraine

Tensor networks provide an effective framework to study many-body problems in strongly-correlated systems, since they can capture the structure of entanglement of the ground state wave function [1]. For two-dimensional quantum systems infinite projected entangled pair states (iPEPS) have proven themselves as an efficient wave-function ansatz capable of representing both symmetry-broken phases and topological orders [2-4]. To represent the entanglement structure of the ground state the PEPS tensor network usually mimics the lattice on which the original model is defined. There are several ways to calculate observables with PEPS tensor network: the corner transfer matrix renormalization group (CTMRG) [5], the boundary matrix product states [6], the tensor renormalization group [7] with CTMRG scheme being the most widely employed. Unfortunately, the CTMRG is usually applied in a straightforward manner only on the square lattice geometry. This initiated the development of various methods to map the original lattice into the square lattice, with the mapping process usually not respecting the original lattice symmetries and possibly enlarging the necessary unit cell [8-11].

We report on a successful application of the generalization of the CTMRG approach to the honeycomb lattice geometry [12,13] with the calculation of relevant physical observables and optimization of the iPEPS wave function directly on the honeycomb lattice. The optimization is realized by means of variational optimization, where gradients are obtained from the automatic differentiation through the CTMRG algorithm. We benchmark our method on both the antiferromagnetic Heisenberg and Kitaev models and obtain the state-of-the-art accuracy of the corresponding results. In particular, the obtained iPEPS are able to capture both symmetry-broken gapless magnetic and the gapless Kitaev spin-liquid states.

We also generalize the theoretical approach to other lattice geometries. For this aim, we have developed the generalization of the CTMRG algorithm to other Archimedean lattices: triangular, kagome, square-octagon, star, ruby, and square-hexagon-dodecahedron. We also report on CTMRG for some non-Archimedean lattices, in particular, the dice lattice. The proposed CTMRG algorithm derivation scheme may also be generalized to even more exotic lattice geometries, like Shastry-Sutherland lattice, maple-leaf, or square-kagome lattices. We have tested the proposed CTMRG methods on the problems of classical statistical mechanics, like the classical two-dimensional Ising models, which can be also formulated in terms of tensor networks. Our results for these classical models are in excellent agreement with the previous numerical and analytical results. Another possible generalization concerns the application of the proposed CTMRG methods to larger unit cells or to problems, which partly break lattice rotational symmetries. In this direction, we were able to generalize the honeycomb CTMRG to two-site unit cells.

The proposed methods open the way to numerous future applications and generalizations. In particular, some of the CTMRG schemes can be naturally used for the optimization of iPEPS with

long-range interactions (up to the 5-th neighbor). This may allow the simulation of systems with fine-tuned flat bands, which are predicted to host various exotic topological orders. Another possible application concerns the calculation of excited states. Even more exotic applications may exist: the CTMRG may be generalized to non-flat lattices, in particular, hyperbolic lattices, which were recently experimentally realized in circuit quantum electrodynamics experiments and which may exhibit completely new phases.

References

1. Orús, R. Tensor networks for complex quantum systems. Nat Rev Phys **1**, 538–550 (2019). https://doi.org/10.1038/s42254-019-0086-7.

2. Corboz, P., Rice, T.M., Troyer, M. Competing States in the *t-J* Model: Uniform *d*-Wave State versus Stripe State. Phys. Rev. Lett. **113**, 046402 (2014). https://doi.org/10.1103/PhysRevLett.113.046402.

3. Lee, C. Y.,Normand, B., Kao, Y.J. Gapless spin liquid in the kagome Heisenberg antiferromagnet with Dzyaloshinskii-Moriya interactions. Phys. Rev. B **98**, 224414 (2018). https://doi.org/10.1103/PhysRevB.98.224414.

4. Hasik, J., Van Damme, M., Poilblanc, D., Vanderstraeten, L. Simulating Chiral Spin Liquids with Projected Entangled-Pair States. Phys. Rev. Lett. **129**, 177201 (2022). https://doi.org/10.1103/PhysRevLett.129.177201.

5. Orús, R., Vidal, G., Simulation of two-dimensional quantum systems on an infinite lattice revisited: Corner transfer matrix for tensor contraction. Phys. Rev. B **80**, 094403 (2009). https://doi.org/10.1103/PhysRevB.80.094403.

6. Jordan, J., Orús, R., Vidal, G., Verstraete, F., Cirac, J. I. Classical Simulation of Infinite-Size Quantum Lattice Systems in Two Spatial Dimensions. Phys. Rev. Lett. **101**, 250602 (2008). https://doi.org/10.1103/PhysRevLett.101.250602.

7. Gu, Z. C., Levin, M., and Wen X. G. Tensor-entanglement renormalization group approach as a unified method for symmetry breaking and topological phase transitions. Phys. Rev. B **78**, 205116 (2008). https://doi.org/10.1103/PhysRevB.78.205116.

8. Corboz, P., Lajkó, M., Läuchli, A. M., Penc, K., and Mila, F. Spin-Orbital Quantum Liquid on the Honeycomb Lattice. Phys. Rev. X **2**, 041013 (2012). https://doi.org/10.1103/PhysRevX.2.041013.

9. Corboz, P., Penc, K., Mila, F., Läuchli, A. M. Simplex solids in $SU(N)$ Heisenberg models on the kagome and checkerboard lattices. Phys. Rev. B **86**, 041106(R) (2012). https://doi.org/10.1103/PhysRevB.86.041106.

10. Jahromi, S.S., Orús, R. Spin-$\frac{1}{2}$ Heisenberg antiferromagnet on the star lattice: Competing valence-bond-solid phases studied by means of tensor networks. Phys. Rev. B **97**, 115161 (2018). https://doi.org/10.1103/PhysRevB.98.155108.

11. Jahromi, S. S., Orús, R., Kargarian, M., Langari, A. Infinite projected entangled-pair state algorithm for ruby and triangle-honeycomb lattices. Phys. Rev. B **97**, 115161 (2018). https://doi.org/10.1103/PhysRevB.97.115161.

12. Gendiar, A., Krcmar, R., Andergassen, S., Daniška, M., Nishino, T. Weak correlation effects in the Ising model on triangular-tiled hyperbolic lattices. Phys. Rev. E **86**, 021105 (2012). https://doi.org/10.1103/PhysRevE.86.021105.

13. Lukin, I. V., Sotnikov A. G. Variational optimization of tensor-network states with the honeycomb-lattice corner transfer matrix. Phys. Rev. B **107**, 054424 (2023). https://doi.org/10.1103/PhysRevB.107.054424.

Free-space quantum channels: Numerical simulations

M. Klen[1,2] and <u>A. A. Semenov</u>[1,2,3]

[1]Bogolyubov Institute for Theoretical Physics, NAS of Ukraine, Vul. Metrologichna 14b, 03143 Kyiv, Ukraine
[2]Kyiv Academic University, Blvd. Vernadskogo 36, 03142 Kyiv, Ukraine
[3]Institute of Physics, NAS of Ukraine, Prospect Nauky 46, 03028 Kyiv, Ukraine

Quantum channels in free space attract great attention from the perspective of their practical applications in many important communication scenarios. For example, they are applied to establish secure communication through hard-to-reach regions, communication with and between moving objects, global satellite-mediated communication, etc. Beyond the task of quantum key distribution, these channels could be used for quantum digital signature, connecting quantum devices with quantum teleportation or entanglement swapping protocols, etc. Atmospheric turbulence is a leading disturbance factor for such channels. Therefore, an accurate theoretical description of its impact on the quantum states of a light mode is important for both fundamental and applied research in quantum optics and quantum communication.

We consider a group of protocols that do not involve the spatial structure of light modes. In this case, the input state at the transmitter is related to the output state at the receiver via the input-output relation,

$$P_{\text{out}}(\alpha) = \int\limits_{0}^{1} \mathrm{d}\eta \, \frac{1}{\eta} P_{\text{in}}\left(\frac{\alpha}{\sqrt{\eta}}\right) \mathscr{P}(\eta), \tag{9.1}$$

see Ref. [1]. Here $P_{\text{in}}(\alpha)$ and $P_{\text{out}}(\alpha)$ are the Glauber-Sudarshan P-functions characterizing the quantum states of a light mode at the transmitter and receiver, respectively. The quantity $\eta \in [0,1]$ describes the channel transmittance, while the function $\mathscr{P}(\eta)$ is the probability distribution of transmittance (PDT). The latter represents the main characteristic of atmospheric quantum channels. The PDT depends on the beam parameters at the transmitter, the channel length, the turbulence parameters, and the receiver characteristics.

Several analytical models for the PDT have been proposed in literature. One of them is focused on the impact of beam wandering [2]. The elliptic-beam model [3] also incorporates beam-spot distortions, which are approximated by Gaussian elliptic beams with randomly oriented semi-axes. The truncated log-normal distribution, discussed in Ref. [4], is applicable in cases where the beam-spot distortion plays a critical role. Furthermore, under the assumption of statistical independence between beam wandering and beam-spot distortion, the PDT can be derived using the law of total probability, as outlined in Ref. [5].

The direct application of analytical models is faced with the problem of properly determining the domain of their applicability. Typically, it is considered to depend on the strength of the turbulence. In this contribution, for details see Ref. [6], we report on numerical simulations of atmospheric quantum channels and use the results for validation of analytical models. This enables, among other applications, to conclude on the range of their applicability.

The random component of the channel transmittance is caused by fluctuations in the index of refraction due to atmospheric turbulence. This, in turn, leads to random fluctuations in the shape of the beam and its fraction passing through the receiver aperture. Considering a classical field with amplitude $u(\mathbf{r}; z)$, the channel transmittance is defined as

$$\eta = \int_{\mathscr{A}} d^2\mathbf{r}|u(\mathbf{r}; z)|^2, \tag{9.2}$$

where $\mathscr{A}$ is the amplitude opening. Thus, to sample the channel transmittance η, it is necessary to first sample the field amplitude $u(\mathbf{r}; z)$ at the aperture plane. We have performed this task with the sparse-spectrum model [7] for the phase-screen method [8].

We have also introduced an empirical model of the PDT based on the beta distribution. This distribution can be parameterized by the moments $\langle \eta \rangle$ and $\langle \eta^2 \rangle$, which can be calculated from the classical theory of optical radiation in the turbulent atmosphere. For a wide range of channel parameters, the beta distribution model provides better agreement with numerical simulations than other analytical models.

Having implemented this method, we studied the three channels with different turbulence impact: weak, moderate and strong. We compared all the mentioned models with simulated PDTs. Our results have shown that the applicability of the analytical models depends mainly on the radius of the receiver aperture and only slightly on the turbulence strength. Our numerical results are applied to study the transmission of non-classical properties of quantum light through free-space channels.

References

1. A. A. Semenov and W. Vogel, Quantum light in the turbulent atmosphere, Phys. Rev. A **80**, 021802 (2009).

2. D. Yu. Vasylyev, A. A. Semenov, and W. Vogel, Toward global quantum communication: Beam wandering preserves nonclassicality, Phys. Rev. Lett. **108**, 220501 (2012).

3. D. Vasylyev, A. A. Semenov, and W. Vogel, Atmospheric quantum channels with weak and strong turbulence, Phys. Rev. Lett. **117** 090501, (2016).

4. Peter W Milonni, John H Carter, Charles G Peterson, and Richard J Hughes, Effects of propagation through atmospheric turbulence on photon statistics, J. Opt. B: Quantum Semiclass. Opt. **6(8)**, S742 (2004).

5. D. Vasylyev, W. Vogel, and A. A. Semenov. Theory of atmospheric quantum channels based on the law of total probability, Phys. Rev. A **97**, 063852 (2018).

6. M. Klen and A. A. Semenov. Numerical simulations of atmospheric quantum channels, Phys. Rev. A **108**, 033718 (2023).

7. M. Charnotskii. Sparse spectrum model for a turbulent phase, J. Opt. Soc. Am. A **30(3)**, 479 (2013).

8. J. A. Fleck, J. R. Morris, and M. D. Feit. Time-dependent propagation of high energy laser beams through the atmosphere, Appl. Phys. **10(2)**, 129 (1976).

Interferometry and coherent dynamics of a superconducting qubit in front of a mirror

Maksym Liul[1], Sergey N. Shevchenko[1]

[1]B. Verkin Institute for Low Temperature Physics and Engineering, Kharkov, Ukraine

A superconducting qubit in a semi-infinite transmission line is an important object in waveguide quantum electrodynamics. The investigation of the considered system could be used for studying many interesting phenomena in this branch of physics such as dynamics in atom-like mirrors, collective Lamb shift, the dynamical Casimir effect, cross-Kerr effect and many others. In our research the qubit is driven periodically (by two signals: probe and pump), what allows to study Landau-Zener-Stuckelberg-Majorana (LZSM) interference [1, 2]. The LZSM interferometry is a fascinating effect which serves for studying fundamental physics and for characterizing and controling of quantum systems. Circuits with superconducting qubits in front of a mirror serve as a good platform to study the dynamics of LZSM interference since they provide the strong coupling between propagating fields and qubits and easy in their fabrication.

In this work we expand the results obtained in Ref. [3], where one can find the detailed description of the experiment. Here we will be focused on the theoretical aspects of the research. The probe (with probe frequency ω_p and probe power P_p) and pump (with pump frequency ω_{pump} and pump power P_{pump}) signals are applied to the transmission line and the on-chip flux line (which modulates the transition frequency of the qubit), respectively. Then the reflection coefficient from the mirror (capacitance) r is measured. Both frequency and power for the pump tone and probe tone are all tunable.

In Ref. [4], the authors associated the reflection coefficient r with the theoretically calculated probability of an upper level occupation P_1 (increasing P_1 corresponds to decreasing r). Here the same correspondence between theory and experiment is used. The system can be described by the Hamiltonian (detailed derivation can be seen in Ref. [4]):

$$H_1 = -\frac{\hbar(\omega_p - \omega_{10}) + \delta \sin \omega_{pump} t}{2} \sigma_z + \frac{\hbar G}{2} \sigma_x. \tag{10.1}$$

Here δ is the amplitude of the energy-level modulation (corresponds to P_{pump} in the experiment), G characterizes the coupling to the probe signal (corresponds to P_p in the experiment), ω_{10} is a qubit frequency. In order to describe the qubit dynamics, we use the Lindblad equation, which in the diabatic basis with the Hamiltonian (10.1) has the form:

$$\frac{d\rho}{dt} = -\frac{i}{\hbar}\left[\widehat{H}_1, \rho\right] + \sum_\alpha \check{L}_\alpha[\rho], \tag{10.2}$$

where $\rho = \begin{pmatrix} \rho_{00} & \rho_{01} \\ \rho_{01}^* & 1 - \rho_{00} \end{pmatrix}$ is the density matrix, such that $P_1 = 1 - \rho_{00}$. The Lindblad superoperator $\check{L}_\alpha$ characterizes the system relaxation caused by interactions with the environment,

$$\check{L}_\alpha[\rho] = L_\alpha \rho L_\alpha^+ - \frac{1}{2}\left\{L_\alpha^+ L_\alpha, \rho\right\}, \tag{10.3}$$
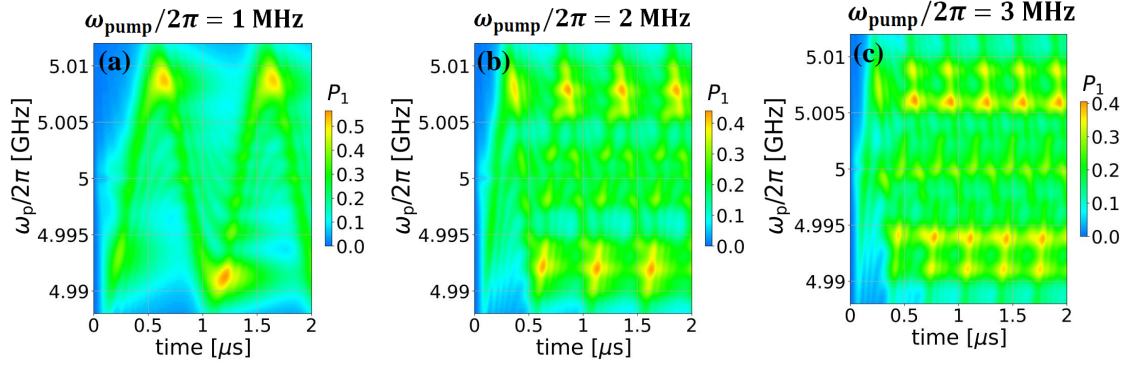
Figure 10.1: Dynamics of the transmon qubit: the upper-level occupation probability P_1 as a function of the probe frequency ω_p and time t, using the probe amplitude $G = 2\pi \times 1.4$ MHz and the pump amplitude $\delta = 10$ MHz. The qubit is irradiated by a pump with frequency (a) $\omega_{pump}/2\pi = 1$ MHz, (b) $\omega_{pump}/2\pi = 2$ MHz, (c) $\omega_{pump}/2\pi = 3$ MHz.

where $\{a,b\} = ab + ba$ is the anticommutator. For a qubit there are two possible relaxation channels: energy relaxation (described by L_{relax}) and dephasing (described by L_ϕ). The corresponding operators can be expressed in the following form:

$$L_{relax} = \sqrt{\Gamma_1}\sigma^+, \quad L_\phi = \sqrt{\frac{\Gamma_\phi}{2}}\sigma_z \tag{10.4}$$

with $\sigma^+ = \begin{pmatrix} 0 & 1 \\ 0 & 0 \end{pmatrix}$, $\sigma_z = \begin{pmatrix} 1 & 0 \\ 0 & -1 \end{pmatrix}$, Γ_1 being the qubit relaxation, $\Gamma_2 = \Gamma_1/2 + \Gamma_\phi$ is the decoherence rate, Γ_ϕ is the pure dephasing rate.

Solving of Eq. (10.2) gives dependence of P_1 on time t, pump frequency ω_{pump}, pump signal amplitude δ, probe frequency ω_p, probe signal amplitude G. The dependence obtained allows us to build, for instance, $P_1 = P_1(\omega_p, t)$. Fig. 10.1 shows such a function for cases (a) $\omega_{pump}/2\pi = 1$ MHz, (b) $\omega_{pump}/2\pi = 2$ MHz, (c) $\omega_{pump}/2\pi = 3$ MHz. Such dependencies were not studied experimentally, therefore all results are obtained theoretically. A good agreement between theory and experiment in Ref. [3] allows us to carry out such and any similar functions. The obtained dependencies may be interesting and useful for setting up future experiments.

Analyzing obtained dependencies one can conclude that, for the case $\omega_{pump}/2\pi = 1$ MHz, the resonance peaks are not distinguished, this may be due to the fact that they are located too close to each other and therefore merge. For Fig. 10.1(b), strong peaks are observed only at a distance $\omega/2\pi = 8$ MHz from the line $\omega_p/2\pi = 5$ GHz, for the case (c) strong peaks are observed only at distances $\omega/2\pi = 6$ MHz, 9 MHz from the line $\omega_p/2\pi = 5$ GHz, while peaks at a distance of $\omega/2\pi = 3$ MHz are weakly pronounced.

Also we can compute the dependencies for P_1 in a stationary regime by making the time averaging of the results (the procedure of averaging is described in Ref. [3]). Figure 10.2 shows a time-averaged interferogram, where P_1 is a function of ω_{pump} and ω_p. We see that with increasing of pump amplitude δ the number of peaks is increasing as well. It is seen that the larger the pump
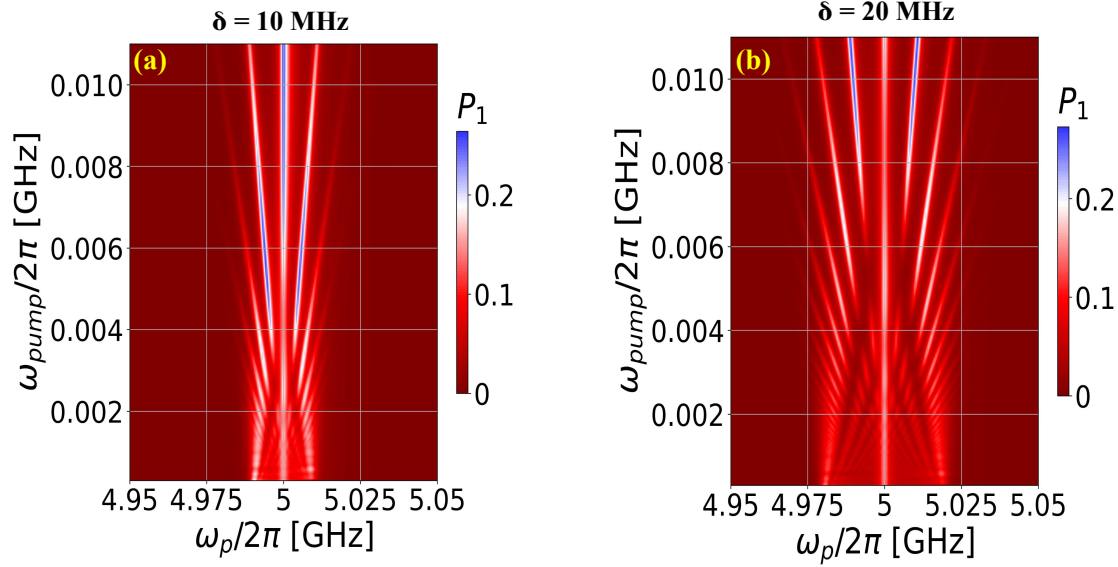
Figure 10.2: LZSM interferograms: the dependence of upper-level occupation probability P_1 on ω_{pump} and ω_p at fixed pump amplitude δ for a weak probe $G = 2\pi \times 0.7$ MHz. Panel (a) corresponds to the pump signal amplitude value $\delta = 10$ MHz, for panel (b) the pump signal amplitude value is $\delta = 20$ MHz.

amplitude δ the larger the amplitude along the ω_p-axis. One can observe similar dependencies in Ref. [4], where only stationary regime was considered.

To summarize, we considered the dynamics and stationary regime of a capacitively shunted transmon-type qubit in front of a mirror, affected by two signals: probe and dressing (pump) signals. The presented dependencies were obtained theoretically, but a good correspondence of developed theory with the experiment in Ref. [3] allows us to assert the correctness of presented results. The obtained dependencies may be interesting and useful for setting up future experiments.

References

1. M. P. Liul, and S. N. Shevchenko, Rate-equation approach for multi-level quantum systems, Low Temp. Phys. **49**, №. 1, 96–102 (2023). DOI: 10.1063/10.0016482

2. M. P. Liul, A. I. Ryzhov, S. N. Shevchenko, Interferometry of multi-level systems: rate-equation approach for a charge qudit, Eur. Phys. J.: Spec. Top. (2023). DOI: 10.1140/epjs/s11734-023-00977-4

3. M. P. Liul, C.-H. Chien, C.-Y. Chen, P. Y. Wen, J. C. Chen, Y.-H. Lin, S. N. Shevchenko, Franco Nori, I.-C. Hoi, Coherent dynamics of a photon-dressed qubit, Phys. Rev. B **107**, №. 19, 195441 (2023). DOI: 10.1103/PhysRevB.107.195441

4. P. Y. Wen, O. V. Ivakhnenko, M. A. Nakonechnyi, B. Suri, J.-J. Lin, W.-J.Lin, J. C. Chen, S. N. Shevchenko, F. Nori, and I.-C. Hoi, Landau-Zener-Stückelberg-Majorana interferometry of a superconducting qubit in front of a mirror, Phys. Rev. B **102**, 075448 (2020). DOI: 10.1103/PhysRevB.102.075448

Separable or Entangled? – How to deduce these quantum ensemble properties from density matrix elements

Gleb Skorobagatko

Institute for Condensed Matter Physics of National Academy of Sciences of Ukraine, Svientsitskii Str. 1, 79011 Lviv, Ukraine

How can one deduce by using only the information about present quantum state of arbitrary open quantum system whether any act of entanglement took place between its counterparts in the system's "history"? - This fundamental question has been debated for more than twenty years in the framework of a modern quantum science [1]. Thus, in order to control the degree of entanglement and/or the effect of interactions between the subsystems of a given quantum system during its time evolution, it is necessary to find proper qualitative measures of the entanglement (or vice versa, separability), which would be encoded in the matrix elements of a given quantum density matrix describing the entire quantum system at arbitrarily chosen moment of time [1–3, 5–9]. As the result, a number of different entanglement (or separability) criteria [1–3, 8–15] has been developed for finite-dimensional quantum density matrices describing composite open quantum systems which are defined in finite-dimensional Hilbert spaces (for the review on different entanglement measures one can see, e.g., Ref. [1]). The search of the most universal and physically transparent forms of separability tests for arbitrary density matrices represents one of the most fundamental challenging problems in the quantum entanglement theory. Besides its fundamental importance the successful solution of this problem can open new perspectives in a wide range of important applications in the area of quantum computation and quantum algorithms optimizations [16-19].

The first important step in such a solution was made in the end of twenty century (in 1996) independently by A. Peres [2] and Horodecki family [3]. This was known in the literature as "Peres-Horodecki (or PPT- positive partial transpose) separability criterion" [1-3]. However, the applicability of the most famous PPT-criterion of separability is restricted by two-qubits density matrices only [2,3] while its general physical background has not been clarified until the appearance of the paper [4]. Especially, the general solution of this common separability problem has been proposed by the author in Ref. [4] where the general physical background behind the Peres–Horodecki positive partial transpose (PPT-) separability criterion has been revealed [4] for the first time. Especially, a general physical sense of partial transpose operation is shown [4] to be equivalent to what one can call as the *"local causality reversal"* (LCR-) procedure for all separable quantum systems, or to the demonstration of *a global time arrow direction uncertainty* in all entangled cases.

The central idea of a novel approach being proposed by the author in Ref. [4] is to circumvent the problem of the ambiguity in the entanglement witnesses construction by analysing instead another general properties which distinguish between separable and entangled quantum states of arbitrary multi-partite quantum system in the most general case. The latter properties are encoded in different causal relations for the ignorance- (meaning the ignorance about the true quantum state of the system) and in virtual quantum transition probabilities for all separable and all entangled cases, correspondingly. These causal relations are shown to be intimately connected with general symmetry of arbitrary separable and arbitrary entangled quantum states with respect to the operation

of *local causality reversal* (for all possible separable states) or with respect to the uncertainty in a global time arrow direction (for all possible entangled states).

In the simplest $2 \otimes 2$ case it is easy to show [2,3] that ppt-separability criterion is equivalent to the requirement of the non-negativity for both following determinants

$$W_1 = \rho_{11|11}^{T_1}\rho_{22|22}^{T_1} - \rho_{11|22}^{T_1}\rho_{22|11}^{T_1}, \qquad W_2 = \rho_{12|12}^{T_1}\rho_{21|21}^{T_1} - \rho_{12|21}^{T_1}\rho_{21|12}^{T_1}, \qquad (11.1)$$

constructed from the matrix elements of a given pt-transformed $2 \otimes 2$ density matrix $\hat{\rho}^{T_1}$ of arbitrary bipartite quantum system, where each among its two subsystems "lives" in the 2-dimensional Hilbert subspace (here $\mu, \nu, n, m = 1, 2$). If both $W_{1,2}$ are non-negative then corresponded density matrix describes separable bipartite quantum system, whereas if either W_1 or W_2 is negative then corresponding bipartite quantum system is entangled (see Refs. [2,3]) .

In the basic author's paper [4] it has been demonstrated for the first time that the ppt criterion for $2 \otimes 2$ density matrices exploiting Eqs. (11.1) contains hints to a more global law of nature which aims to connect a new universal separability criterion for arbitrary density matrices with very general causal and probabilistic considerations. This brand new causal probabilistic law – *universal causal separability criterion* (UCSC) – has been revealed for the first time in Ref. [4].

The respective two universal causal probabilistic relations connect probabilities of observer's ignorance about j-th configuration of states for arbitrary composite system $P_{\varnothing}^{(j)}$ and $P_{-\varnothing}^{(j)}$ – when the *global time arrow is reversed* – with the probability $P_{\circlearrowleft}^{(j)}$ of a virtual quantum transition for j-th configuration of composite quantum system's base states and with the probability $P_{\circlearrowright}^{(j)}$ of the same kind of virtual quantum transition for the j-th configuration of the system while the *local causality reversal* procedure is implemented to any among subsystems of a given composite quantum system [4]. From Eqs. (11.1) one can deduce that these two fundamental causal probabilistic relations should have different forms for arbitrary separable and arbitrary entangled states of any composite quantum system [4]. Especially, in all separable cases of any kind one should have [4]

$$P_{\varnothing}^{(j)} = P_{\circlearrowleft}^{(j)} + P_{\circlearrowright}^{(j)}. \qquad (11.2)$$

At the same time, in all entangled situations one should have [4]

$$P_{\circlearrowleft}^{(j)} = P_{\varnothing}^{(j)} + P_{-\varnothing}^{(j)}. \qquad (11.3)$$

One can also see these symmetries and related causal considerations on Fig. 11.1 for both separable (left picture) and entangled (right picture) cases.

Physically, Eqs. (11.2) and (11.3) reflect two different causal symmetries: i) *the probability of observer's ignorance about the quantum state of separable constituent subsystems of quantum system during its preparation is invariant with respect to the local causality reversal (LCR-) procedure performed on any separable subsystem of a given quantum system* for Eq. (11.2) and ii) *the probability of a virtual quantum transition between two completely orthogonal compositions of base states of the entangled quantum system – remains invariant with respect to a reversal of a global time arrow* for Eq. (11.3) correspondingly (see Ref. [4]).
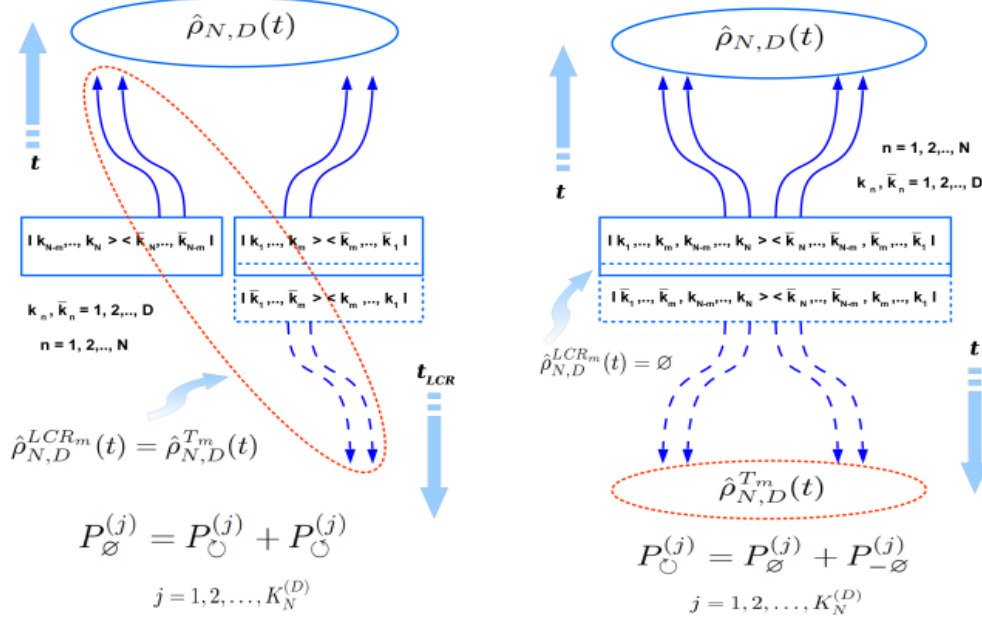
Figure 11.1: Left: Schematic picture of the evolution of density matrix defined in $D^{\otimes N}$ Hilbert space (encoding N quantum subsystems of D eigenstates each) in the *separable case* with respect to the *local causality reversal* (LCR-) procedure performed on m among N its subsystems ($m = 1, 2, \ldots N - 1$). Right: Schematic picture of the evolution of density matrix defined in $D^{\otimes N}$ Hilbert space (encoding N quantum subsystems of D eigenstates each) in the *entangled case* with respect to two possible directions of a global time arrow and pt-transformation performed on m among N its constituent subsystems ($m = 1, 2, \ldots N - 1$).

Now in order to complete the definition of a brand new *universal causal separability criterion* (UCSC) one needs to specify all terms from Eqs. (11.2) and (11.3) for the most general situation of density matrix of arbitrary dimensionality encoding arbitrary ensemble of $N \geq 2$ similar (either interacting or not with each other) quantum subsystems of the dimensionality $D \geq 2$ of each subsystem's Hilbert subspace [4]. Thus, the dimensionality of the entire density matrix Hilbert space should be $D^N \geq 4$ (or less for the cases of strongly interacting quantum ensembles). Remarkably, the resulting universal separability criterion (UCSC) should give correct predictions for both finite and infinite integer numbers D and N.

To complete this program it is quite natural [4] to define an arbitrary base state vector of the entire $D^{\otimes N}$ quantum system as its (j-th) configuration

$$|\{k_N\}^{(j)}\rangle = \prod_{n=1}^{N} \otimes |k_n^{(j)}\rangle \tag{11.4}$$

with $k, k' = 1, .., D; \; j = 1, .., K_N^{(D)}$.

Then one can introduce a *completely orthogonal configuration* of the state vectors of subsystems with respect to its arbitrarily chosen j-th configuration as the base vector of state of the entire sys-

tem being completely orthogonal to a vector of state for chosen j-th system configuration $|\{k_N\}^{(j)}\rangle$. This yields

$$|\{\bar{k}_N\}^{(l)}\rangle = \prod_{n=1}^{N} \otimes |k_n'^{(l)}\rangle_{(k \neq k'),(j \neq l)}.$$
(11.5)

For the total number of all distinct configurations one has [4]

$$K_N^{(D)} = \left\{ \frac{1}{\left[\frac{1}{D^N} + \left(1 - \frac{1}{D}\right)^N \right]} \right\}_{in}$$
(11.6)

here the symbol $\{\ldots\}_{in}$ means integer part of the number. Therefore, in the basis of orthonormal state vectors of Eq.(5) (or equally, in the basis of *all system's configurations*) arbitrary density matrix $\hat{\rho}_N^{(D)}$ defined in the $D^{\otimes N}$ Hilbert space takes following form [4]

$$\hat{\rho}_N^{(D)} = \sum_{j,j'=1}^{D^N} |\{k_N\}^{(j)}\rangle \rho_{\{k\}_j|\{k\}_{j'}} \langle \{k_N\}^{(j')}|,$$
(11.7)

where each among summation indices j, j' runs all D^N possible configurations of the entire quantum system [4].

Using Eqs. (11.2)–(11.7), one can deduce for the "ignorance probability" $P_\varnothing^{(j)}$, which reflects the uncertainty in observer's knowledge about the realization of either $\{k_N\}^{(j)}$ configuration or one among its completely orthogonal $\{\bar{k}_N\}^{(j)}$ counterparts in given arbitrary N-partite quantum system from $D^{\otimes N}$ Hilbert space a following formula

$$P_\varnothing^{(j)} = \rho_{\{k\}_j|\{k\}_j} \left(\sum_{l=1}^{N_{o.c.}} \rho_{\{\bar{k}\}_l|\{\bar{k}\}_l} \right),$$
(11.8)

where $N_{o.c.}$ is the number of completely orthogonal configurations $\{\bar{k}_N\}^{(l)}$ for given configuration $\{k_N\}^{(j)}$ chosen, $N_{o.c.}$ is different in the cases of non-interacting and interacting subsystems in the ensemble [4].

Analogously, for the probability $P_\circlearrowleft^{(j)}$ of a virtual quantum transition for the arbitrary distinct configuration of the entire quantum system living in the $D^{\otimes N}$ Hilbert space involving its completely orthogonal counterparts $\{k\}_j$ and $\{\bar{k}\}_l$ one has

$$P_{\circlearrowleft(m)}^{(j)} = \sum_{l=1}^{N_{v.t.}} \rho_{\{k\}_j|\{\bar{k}\}_l}^{T_m} \rho_{\{\bar{k}\}_l|\{k\}_j}^{T_m},$$
(11.9)

where the symbol ρ^{T_m} means the operation of partial transposition of a density matrix $\hat{\rho}$ simultaneously in the m ($m \leq (N-1)$) subspaces of its Hilbert space.

Therefore, new definitions (11.8) and (11.9) for the ignorance- and virtual quantum transition probabilities for arbitrary density matrices of the rank $\leq D^N$ allow one to find the explicit form of

the probabilities $P^{(j)}_{\circlearrowleft(m)} = W^{(j)}_m$ and $P^{(j)}_{-\varnothing(m)} = -W^{(j)}_m$ for all separable- and for entangled situations of Eqs. (11.2) and (11.3), respectively. In both these situation one has for the quantity $W^{(j)}_m$ a following general formula (see Ref. [4])

$$W^{(j)}_m = \left(\rho_{\{k\}_j | \{k\}_j} \sum_{l=1}^{N_{o.c.}} \rho_{\{\bar{k}\}_l | \{\bar{k}\}_l} \right) - \left(\sum_{l=1}^{N_{v.t.}} \rho^{T_m}_{\{k\}_j | \{\bar{k}\}_l} \rho^{T_m}_{\{\bar{k}\}_l | \{k\}_j} \right). \tag{11.10}$$

In Eq. (11.10) the integer number $K^{(D)}_N$ is a number of all distinct (i.e. not completely orthogonal) configurations of the ensemble of N D-dimensional quantum subsystems joined into one either interacting (coupled) or not quantum ensemble, whereas in different (interacting or not) situations one has for integer numbers $N_{o.c.}$ and $N_{v.t.}$ in Eq. (11.10) following different (dual) relations (see Ref. [4])

$$\begin{cases} N_{o.c.} = (D-1)^N, & N-free\ ensemble \\ N_{o.c.} = (D-1), & N-coupled\ ensemble \end{cases} \tag{11.11}$$

and

$$\begin{cases} N_{v.t.} = (D-1), & N-free\ ensemble \\ N_{v.t.} = (D-1)^N, & N-coupled\ ensemble \end{cases} \tag{11.12}$$

In Eqs. (11.11) and (11.12) the terms $N-coupled$ (and $N-free$) mark two opposite situations where all N quantum subsystems of the ensemble are interacting (non-interacting) with each other at the moment of time when one measures matrix elements of a given density matrix of the ensemble [4].

Hence, from Eqs. (11.8)–(11.12) for *each j-th* distinct configuration $\{k\}_j$ of N subsystems' base quantum states one has the following general form of the *universal causal separability criterion* (UCSC) [4]

$$W^{(j)}_m = \begin{cases} P^{(j)}_{\circlearrowleft(m)}, & for\ W^{(j)} \geq 0, \quad if\ \{k_N\}^{(j)}\ is\ m-separable; \\ -P^{(j)}_{-\varnothing(m)}, & for\ W^{(j)} < 0, \quad if\ \{k_N\}^{(j)}\ is\ m-entangled. \end{cases} \tag{11.13}$$

For arbitrary density matrix defined in $D^{\otimes N}$ Hilbert space there exist $K^{(D)}_N$ separability/entanglement conditions of the type (11.10)–(11.13) – one for each among $K^{(D)}_N$ distinct configuration of subsystems' eigenstates. Some of these equations may appear to be equal to each other, thus, sufficiently reducing the total number of restrictions system should obey to be separable/entangled.

Resulting general formulas have been then analyzed in details in paper [4] for the widest specific type of one-parametric density matrices of arbitrary dimensionality, those modelling a number N of equivalent quantum subsystems of a dimensionality D in each subsystem's Hilbert subspace, being all equally connected (EC-) with each other to arbitrary degree by means of a single entanglement parameter $0 \leq p \leq 1$ (see Ref. [4]). As the result, a number of remarkable features of the entanglement thresholds $p_{th}(D,N)$ for such EC-density matrices have been described for

the first time in Ref. [4]. This includes, especially, different kinds of "separability windows" on the entangled backgrounds, remarkable dualities in separability/entanglement properties between different limiting cases on the parameter p values (see Ref. [4] for details). All novel results being obtained for the family of arbitrary EC-density matrices are shown to be applicable to a wide range of both interacting and non-interacting (at the moment of measurement) multi-partite quantum systems, such as arrays of qubits, spin chains, ensembles of quantum oscillators, strongly correlated quantum many-body systems, etc. (one can see Ref. [4] for further details).

References

1. Horodecki R., Horodecki P., Horodecki M., Horodecki K., Rev. Mod. Phys. **81**, 865 (2009).

2. Peres A., Phys. Rev. Lett. **77**, 1413–1415 (1996).

3. Horodecki M., Horodecki P., Horodecki R., Phys. Lett. A **223 (1–2)**, 1–8 (1996).

4. Skorobagatko G., Sci. Rep. **11**, 15866 (2021).

5. Friis N., Vitagliano G., Malik M. *et al.*, "Entanglement certification from theory to experiment", Nat. Rev. Phys. **1**, 72–87 (2019).

6. Erhard M., Krenn M., Zeilinger A., "Advances in high-dimensional quantum entanglement", Nat. Rev. Phys. **2**, 365–381 (2019).

7. J. Barreiro, T.C. Wei, P. Kwiat, "Beating the channel capacity limit for linear photonic superdense coding" Nature Phys. **4**, 282-286 (2008).

8. R. Simon, "Peres-Horodecki Separability Criterion for Continuous Variable Systems", Phys. Rev. Lett. **84**, 2726 (2000).

9. R.F. Werner, "Quantum states with Einstein-Podolsky-Rosen correlations admitting a hidden-variable model", Phys. Rev. A **40**, 4277 (1989).

10. C. Spengler, M. Huber, S. Brierley, T. Adaktylos, B.C. Hiesmayr, "Entanglement detection via mutually unbiased bases", Phys. Rev. A **86**, 022311 (2012).

11. R.A. Bertlmann, K. Durstberger, B.C. Hiesmayr, P.Krammer, "Optimal entanglement witnesses for qubits and qutrits", Phys. Rev. A **72**, 052331 (2005).

12. Y. Zhong, H.S. Chang, A. Bienfait *et al.*, "Deterministic multi-qubit entanglement in a quantum network", Nature **590**, 571–575 (2021).

13. S. Gerke, W. Vogel, J. Sperling, "Numerical Construction of Multipartite Entanglement Witnesses", Phys. Rev. X **8**, 031047 (2018).

14. M. Fadel, A. Usui, M. Huber, N. Friis, G. Vitagliano, "Entanglement Quantification in Atomic Ensembles", Phys. Rev. Lett. **127**, 010401 (2021).

15. D.Sauerwein, N.R.Wallach, G.Gour, B.Kraus, "Transformations among Pure Multipartite Entangled States via Local Operations are Almost Never Possible", Phys. Rev. X **8**, 031020 (2018).

16. B.Bergh, M.Gärttner, "Experimentally Accessible Bounds on Distillable Entanglement from Entropic Uncertainty Relations", Phys. Rev. Lett. **126**, 190503 (2021).

17. N. Kalb, A.A. Reiserer, P.C. Humphreys *et al.*, "Entanglement distillation between solid-state quantum network nodes", Science **546**, 928-932 (2017).

18. D. Gross, J. Eisert, N. Schuch, D.Perez-Garcia, "Measurement-based quantum computation beyond the one-way model", Phys. Rev. A **76**, 052315 (2007).

19. G.J. Mooney, C.D. Hill, L.C.L. Hollenberg, "Entanglement in a 20-Qubit Superconducting Quantum Computer", Sci. Rep. **9**, 13465 (2019).

Many-body correlations and ordered phases of cold alkaline-earth atoms in state-dependent optical lattices

Andrii Sotnikov[1,2]

[1]Kharkiv Institute of Physics and Technology, Kharkiv, Ukraine
[2]V.N. Karazin Kharkiv National University, Svobody Square 4, 61022 Kharkiv, Ukraine

We explore the rich nature of correlations in the ground state and ordered phases of ultracold atoms trapped in state-dependent optical lattices. In particular, we consider interacting fermionic ytterbium or strontium atoms, realizing a two-orbital Hubbard model with two spin components,

$$\mathscr{H} = \sum_{\langle ij \rangle} \sum_{\gamma,\sigma} t_\gamma (c^\dagger_{i\gamma\sigma} c_{j\gamma\sigma} + \text{H.c.}) - \sum_{i,\gamma} \mu_\gamma n_{i\gamma} + \mathscr{H}_{\text{int}},$$

where

$$\mathscr{H}_{\text{int}} = \sum_{i,\gamma} U_{\gamma\gamma} \sum_{\sigma<\sigma'} n_{i\gamma\sigma} n_{i\gamma\sigma'} + V \sum_{i,\sigma<\sigma',\gamma<\gamma'} n_{i\gamma\sigma} n_{i\gamma'\sigma'}$$
$$+ (V - V_{\text{ex}}) \sum_{i,\sigma,\gamma<\gamma'} n_{i\gamma\sigma} n_{i\gamma'\sigma} + V_{\text{ex}} \sum_{i,\sigma<\sigma',\gamma<\gamma'} c^\dagger_{i\gamma\sigma} c^\dagger_{i\gamma'\sigma'} c_{i\gamma\sigma'} c_{i\gamma'\sigma}.$$

The indices $\gamma, \gamma' = \{g, e\}$ and $\sigma, \sigma' = \{\uparrow, \downarrow\}$ denote the orbital states and the nuclear Zeeman spin states, respectively. The operator $c^\dagger_{i\gamma\sigma}$ ($c_{i\gamma\sigma}$) creates (annihilates) an atom in the internal state $|\gamma\sigma\rangle$ at the site i and the notation $\langle ij \rangle$ means summation over the nearest-neighbor lattice sites only. The local density operator of atoms in the orbital state γ is $n_{i\gamma} = \sum_\sigma n_{i\gamma\sigma}$ and $n_{i\gamma\sigma} = c^\dagger_{i\gamma\sigma} c_{i\gamma\sigma}$. For a particular orbital state γ, t_γ is the hopping amplitude and μ_γ is the chemical potential. The sketch of the system under study is shown in the figure below.
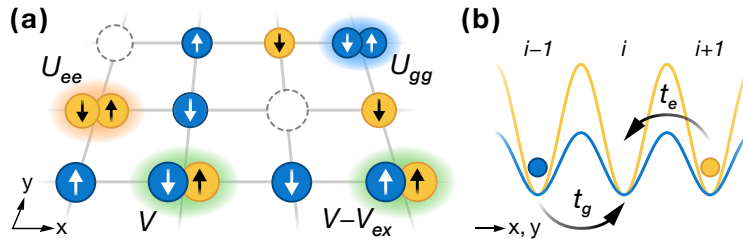
We perform theoretical analysis of the model with the experimentally relevant hierarchy of tunneling and interaction amplitudes. In particular, in one-dimensional setting we employ the exact diagonalization and matrix product states approaches [1]. The band-structure calculations (similar to those performed in Ref. [2]]) with the choice of parameters for the optical lattice with $V_x^{(g)} = 5E_r$ and $V_x^{(e)} = 10.5E_r$ (E_r is the recoil energy of an atom) result in the values of the Hubbard parameters summarized in the table below.

	$t_g(h\times\text{Hz})$	t_e	U_{gg}	U_{ee}	V	V_{ex}
^{173}Yb	160.1	0.2591	9.238	18.13	37.031	25.646
^{171}Yb	161.9	0.2591	0	6.157	15.005	-3.363
^{87}Sr	277.7	0.2591	4.16	9.727	5.724	2.439

We calculate the on-site double occupancy D_{gg} of g atoms, which can be viewed as the global observable easily accessible in the experiments with ultracold multicomponent fermionic mixtures in the lattice. In particular, this can be detected for AEAs using a photoassociation resonance on the $^1S_0 \rightarrow{}^3P_1$ intercombination line. Two atoms can form a bound pair by absorbing a photon when the light is resonant with a bound state of the electronically excited molecule. Due to the short lifetime of the excited molecule, it will eventually decay and the released energy will cause a loss of the atom pair from the trap. This observable is theoretically determined as $D_{gg} = \frac{1}{L}\sum_i \langle n_{ig\uparrow}n_{ig\downarrow}\rangle$.

We observe that D_{gg} can be viewed as a good indicator of the onset of nearest-neighbor magnetic correlations in gases of ^{173}Yb or ^{87}Sr atoms, while for ^{171}Yb there is no such correspondence.

We also analyze the density-wave modulation by calculating the site-averaged amplitude, $\Delta n = \frac{1}{L}\sum_{i,\gamma}|\langle n_{i\gamma}\rangle - n_\gamma|$. This quantity can also be measured in cold-atom systems by using an additional superlattice potential. According to our theoretical analysis, it demonstrates a different behavior to the double occupancy. As we will see below, its enhancement can be used as an additional indicator of the orbital correlations (^{171}Yb and ^{173}Yb), while its suppression can be attributed to the onset of antiferromagnetic correlations in the Mott-insulating regimes with $n = 1$ or $n = 2$ (^{87}Sr and ^{173}Yb).

Next, let us discuss features of the nearest-neighbor correlators, i.e., the spin-spin $\langle \mathbf{S}_i \cdot \mathbf{S}_{i+1}\rangle$ and orbital-orbital $\langle T_i^z T_{i+1}^z\rangle$ ones. These quantities can be experimenatally measured by means of the quantum gas microscope techniques developed for alkaline-earth(-like) atoms. The local spin operator contains contributions from both orbital flavors, $\mathbf{S}_i = \mathbf{S}_{ig} + \mathbf{S}_{ie}$, where the orbital components $\mathbf{S}_{i\gamma} = (S_{i\gamma}^x, S_{i\gamma}^y, S_{i\gamma}^z)$ are expressed in terms of conventional spin-1/2 Pauli matrices as $S_{i\gamma}^r = \frac{1}{2}c_{i\gamma\tau}^\dagger \sigma_{\tau\tau'}^r c_{i\gamma\tau'}$ for $r = (x,y,z)$. In turn, the orbital correlator is defined in terms of the operator $T_i^z = \frac{1}{2}\sum_{\tau=\uparrow,\downarrow}c_{i\gamma\tau}^\dagger \sigma_{\gamma\gamma'}^z c_{i\gamma'\tau}$. The obtained dependencies of the site-averaged spin-spin correlators $\langle \mathbf{S}_i \cdot \mathbf{S}_{i+1}\rangle$ and $\langle S_i^z S_{i+1}^z\rangle$ on the densities of g and e atoms. One can observe that in case of ^{173}Yb, the correlator $\langle S_i^z S_{i+1}^z\rangle$ reveals the antiferromagnetic ordering along diagonals $n_g + n_e = 1$ and $n_g + n_e = 2$, which is manifested by the negative value of $\langle \mathbf{S}_i \cdot \mathbf{S}_{i+1}\rangle$. Note that particularly in these regions we observe a strong suppression of the double occupancy D_{gg}. In turn, the ^{87}Sr system exhibits weaker antiferromagnetic (AFM) correlations along the same diagonals as ^{173}Yb due to lower values of the interaction parameters, but with a similar correspondence in suppression of the D_{gg} signal. Surprisingly, a gas of ^{171}Yb atoms with the AFM on-site Hund's coupling ($V_{ex} < 0$) does not demonstrate any AFM correlations at $n_g \approx n_e \approx 1$. The reason for that originates from the different hierarchy of the interaction amplitudes and thus a different ground state in the strong-coupling limit.

One can also notice that for both isotopes with ferromagnetic Hund's coupling (^{173}Yb and ^{87}Sr with $V_{ex} > 0$) there are certain regimes with a strong FM signal in the correlator $\langle \mathbf{S}_i \cdot \mathbf{S}_{i+1}\rangle$. This FM signal is almost absent in the correlator $\langle S_i^z S_{i+1}^z\rangle$ due to the constraint for finite size and zero total polarization, $N_\uparrow = N_\downarrow$. In turn, due to the AFM exchange interaction ($V_{ex} < 0$) in the ^{171}Yb system, no ferromagnetic correlations develop, which also results into direct correspondence between the depicted spin-spin correlators $\langle \mathbf{S}_i \cdot \mathbf{S}_{i+1}\rangle$ and $\langle S_i^z S_{i+1}^z\rangle$ in the whole diagram.

Therefore, the fillings n_g and n_e, as well as the type of atomic isotope, determine four different magnetic orderings, that we denote AFM-1 ($n_g + n_e \approx 1$), AFM-2 ($n_g + n_e \approx 2$), AFM-3 ($n_g + n_e \approx$

3) and FM. We performed additional calculations in the regions $n_e > 1$ (not shown in figures), which demonstrate that the spin-spin (as well as orbital-orbital) correlators are symmetric with respect to reflections from the line $(n_g + n_e) = 2$. This fact is directly related to the particle-hole symmetry in both orbital flavors and can be useful for verification and control purposes.

The dependencies of the orbital-orbital correlators $\langle T_i^z T_{i+1}^z \rangle$ on the average densities of g and e atoms are also nontrivial. In the case of ^{173}Yb, one can observe antiferroorbital (AFO) ordering around $n_g = 1$ and $n_e = 0.5$, which is manifested by negative correlations. Remarkably, the position and extent of this phase is in a good agreement with the previous mean-field studies of quasi-2D lattice systems [2]. The main feature of the AFO phase is the alternating occupation of neighboring lattice sites by atoms in different orbital states. Note that the AFO-like density modulations also emerge in the case of a gas of strontium atoms with the corresponding maximum of the signal at $n_g = 1$ and $n_e = 0.5$, but with a lower magnitude. It is worth mentioning that the sharp transition features in the dependencies of $\langle T_i^z T_{i+1}^z \rangle$ for ^{173}Yb and ^{171}Yb at $n \approx 1$, $n \approx 1.5$, and $n \approx 2$, as well as in the density-related local correlators, correspond to the transitions to the insulating regimes with the charge gap, which take place also in the thermodynamic limit.

Let us also discuss the dependence of the correlator $\langle T_i^z T_{i+1}^z \rangle$ for the case of ^{171}Yb isotope. In contrast to ^{173}Yb and ^{87}Sr atomic systems, one observes the strongest AFO signal at $n_g = n_e = 1$. AFO-2 is a bipartite ordering similar to AFO-1. However, the main difference is that the neighboring lattice sites are occupied alternately by pairs of g or e atoms. The reason for the AFO instability (which completely suppresses the AFM correlations) in this particular regime for ^{171}Yb system originates from the different hierarchy of the interaction amplitudes and thus a different ground state in the strong-coupling limit [1]. Let us also note that the AFO correlations are usually accompanied by sizeable density modulations (the charge-density wave) on the nearest-neighbor lattice sites.

By employing a dynamical mean-field theoretical analysis, we extend the description of systems to quasi-two-dimensional and three-dimensional state-dependent optical lattices and study low-temperature phases in multicomponent gases of fermionic alkaline-earth(-like) atoms [2,3]. Using the example of ^{173}Yb atoms, we show that a two-orbital mixture with two nuclear spin components is a promising candidate for studies of not only magnetic but also staggered orbital ordering peculiar to certain solid-state materials. We calculate and study the phase diagram of the full Hamiltonian with parameters similar to existing experiments and reveal an antiferro-orbital phase. This long-range-ordered phase is inherently stable, and we analyze the change of local and global observables across the corresponding transition lines, paving the way for experimental observations. Furthermore, we suggest a realistic extension of the system to include and probe a Jahn-Teller source field playing one of the key roles in real crystals.

References

1. V. Bilokon, E. Bilokon, M.C. Bañuls, *et al.*, Many-body correlations in one-dimensional optical lattices with alkaline-earth(-like) atoms. Sci. Rep. **13**, 9857 (2023).

2. A. Sotnikov, N. Darkwah Oppong, Y. Zambrano, and A. Cichy, Orbital ordering of ultracold alkaline-earth atoms in optical lattices. Phys. Rev. Research **2**, 023188 (2020).

3. A. Sotnikov, Y. Zambrano, and A. Cichy, Low-temperature phases in two-orbital Hubbard model realized with ultracold atoms in optical lattices, Acta Phys. Pol. A **138**, 669 (2020).

Semiclassical limit of quantum logic and information loss

Maksym Teslyk[1], Olena Teslyk[2]

[1]Fysisk institutt, UiO, Oslo, Norway
[2]Faculty of Physics, TSNUK, Kyiv, Ukraine

Introduction

As Feynman mentioned in 1982, quantum systems cannot be imitated by classical computing machines [1]. The greatest interest to quantum computers appeared in 1994, after the discovery of Shor's factoring algorithm [2]. Since then a lot has been done in the field, and today both industry and academic institutes are investing a lot to quantum information processing and computation.

Despite that, the origin of quantum calculation efficiency still seems to be a challenge. Both superposition principle and linearity of unitary operators are widely believed to be responsible for the advantage of quantum algorithms. Unfortunately, these might conflict with the Gottesmann-Knill theorem.

Also, one may consider quantum entanglement, which has no classical analog, as another possible solution to the problem. Indeed, it violates Bell's inequalities and is crucial for the implementation of various quantum information transfer protocols. However, its role can also be argued [3,4].

In this study, we analyze the problem from the perspective of propositional logic [5]. Within the approach, any calculation can be interpreted as some logical expression Γ_A which can be either true or false, depending on whether a system possesses some property A. In terms of the classical Boolean logic, this implies dealing with characteristic functions χ_λ determined on the system's phase space $\mathbb{P}$. For example, classical conjunction $\wedge$ (logical AND) of two statements can be represented as

$$\chi_\wedge = \chi_A \wedge \chi_B = \chi_A \chi_B, \tag{13.1}$$

where χ_A and χ_B are characteristic functions encoding the corresponding statements. Together with the negation (logical NOT) and implication, this specifies the complete set of classical logic gates for the Boolean logic.

While dealing with quantum logic, one should use the relevant projector operators P_A from the Hilbert space $\mathbb{H}$ instead. Each such operator projects the system's state $|\psi\rangle$ with the non-zeroth norm onto the corresponding Hilbert subspace. Here, the presence of non-zeroth eigenvector of the operator equals to the TRUE outcome of our proposition. This can be written as

$$P_A |\psi\rangle = |A\rangle \langle A | \psi\rangle. \tag{13.2}$$

Model description

From (13.2) one infers that $P_A |\psi\rangle = 0 \Leftrightarrow \langle A | \psi\rangle = 0$. This resembles a typical behavior of characteristic functions. Within the path integral formalism, one can easily derive the semi-classical limit

for the transition amplitude $\langle A \,|\, \psi \rangle$, namely

$$\lim_{\hbar \to 0} \frac{\hbar}{i} \langle A \,|\, \psi \rangle = \chi_{A|\psi} S, \qquad \chi_{A|\psi} = \begin{cases} 1, & \delta S_{A|\psi} = 0 \\ 0, & \delta S_{A|\psi} \neq 0, \end{cases} \tag{13.3}$$

where $S_{A|\psi}$ stands for the relevant system's action, and $\delta S_{A|\psi}$ is its variation. Eq. (13.3) clearly establishes the interconnection between P_A acting on $|\psi\rangle$ and the relevant characteristic function χ_A. Following the same protocol, we arrive at the quantum-classical interrelation for any gate from the complete set. This covers the non-Abelian case also.

During the semiclassical transition, all possible trajectories reduce to the single one, which describes the classical evolution in $\mathbb{P}$. That means that all information about these trajectories washes out under the limit $\hbar \to 0$. This loss can be estimated with the help of information entropy.

As known, in the quantum case one should deal with the von Neumann entropy. For any pure quantum state it equals to 0. So, for the expression (13.2) one derives the zeroth entropy. However, after the limit $\hbar \to 0$ one should deal with the characteristic function χ_A splitting the phase space onto two distinguishable domains. This allows to introduce the Shannon entropy as

$$H_{\text{Sh}}(\chi_A) = -p_A \ln p_A - (1 - p_A) \ln (1 - p_A) \leq \ln 2. \tag{13.4}$$

Here, $p_A = \int_{\mathbb{P}} \mathscr{D}x \chi_A / \int_{\mathbb{P}} \mathscr{D}x$ stands for the fraction of phase space $\mathbb{P}$ governed by χ_A. The emerging entropy for any projector operator heralds the loss of computational efficiency under the transition from quantum proposition to its classical counterpart.

For any non-commuting operators P_A, P_B: $P_A P_B - P_B P_A = i\hbar \Pi$, where Π is Hermitian, one should take into account that any non-Abelian behavior disappears in the classical case. This requires taking the partial trace over the degrees of freedom governed by Π, thus resulting in a mixed state with some density matrix ρ and the non-zeroth von Neumann entropy

$$H_{\text{N}}(\rho) = -\text{Tr}\,\rho \ln \rho \leq \ln \dim \Pi. \tag{13.5}$$

Here, $\dim \Pi$ determines the number of Hilbert space dimensions of the operator Π. Also, each possible eigenvector of Π contributes as a separate run to the total entropy $H(\chi_{\wedge, \Pi})$ for either product or conjunction. Counting this as the Shannon entropy from the relevant conditional distribution, we arrive at the following expression

$$H(\chi_{\wedge, \Pi}) = H_{\text{N}}(\rho) + \sum_{\pi}^{\dim \Pi} |\langle \psi \,|\, \pi \rangle|^2 H_{\text{Sh}}(\chi_{AB|\pi}), \tag{13.6}$$

where $H_{\text{N}}(\rho)$ is governed by (13.5), and $|\pi\rangle$ is the eigenvector of Π. Quantity $H_{\text{Sh}}(\chi_{AB|\pi})$ stands for the Shannon entropy (13.4) with the fraction $p_{AB|\pi} = \int \mathscr{D}x \chi_{A|\pi} \chi_{B|\pi} / \int \mathscr{D}x$ for the corresponding conditional distribution. Note that the input should be $|\pi\rangle$ instead of $|\psi\rangle$.

Information loss $H(\mathbb{E}\,|S\rangle)$ of some general quantum logical expression $\mathbb{E}$ can be estimated as follows [6]

$$H(\mathbb{E}\,|S\rangle) = \sum_{i=1}^{q} H\left(\chi_{\Gamma_{A_i}}\right) + H(\chi_{\wedge, \Pi_1}) + \sum_{\pi_1}^{\dim \Pi_1} |\langle \psi \,|\, \pi_1 \rangle|^2 H\left(\chi_{\wedge, \Pi_2 | \pi_1}\right)$$

$$\leq (q + c) \ln 2 + \sum_{k=1}^{c} \ln \dim \Pi_k. \tag{13.7}$$

Here, q stands for the number of qubits involved in no conjunction, and the operators emerging from the corresponding commutators are denoted by $\Pi_n, n = \overline{1, c}$, where c is the number of conjunctions.

The obtained results were illustrated by the analysis of two different algorithms: the quantum discrete Fourier transform and the Grover search algorithm. As known, their classical counterparts require $\mathscr{O}(n2^n)$ and $\mathscr{O}(2^n)$ number of steps, respectively; here, n is the number of involved qubits (or bits). Within the approach, the estimated information loss equals to $\mathscr{O}(n2^n)$ for the first algorithm and to $\mathscr{O}\left(n^2 2^{n/2}\right)$ for the second one.

Conclusions

We studied in details how quantum logic can be reduced under the semiclassical limit to its classical counterpart. We estimated the emerging information loss for each elementary gate from the complete set. The proposed technique is generalized to any quantum logical expression. The largest loss is observed for non-commuting operators. As shown in [7], quantum algorithm may experience changeover under the limit $\lim_{\hbar \to 0}$. And this can be clearly estimated with the developed technique; this also demonstrates that our method differs from the Kolmogorov complexity approach [8].

References

1. Feynman, R. P. Simulating Physics with Computers. Int. J. Theor. Phys. **21**, 467-488 (1982). https://doi.org/10.1007/BF02650179.

2. Shor, P. W. Algorithms for quantum computation: discrete logarithms and factoring. Proc. 35th ASFCS, 124-134 (1994). http://dx.doi.org/10.1109/sfcs.1994.365700.

3. Jozsa, R. and Linden, N. On the role of entanglement in quantum-computational speed-up. Proc. R. Soc. Lond. A. **459**, 2011–2032 (2003). https://doi.org/10.1098/rspa.2002.1097.

4. Kendon, V. M. and Munro, W. J. Entanglement and Its Role in Shor's Algorithm. Quantum Info. Comput. **6**, 630-640 (2006).

5. Birkhoff, G. and von Neumann, J. The Logic of Quantum Mechanics. Ann. Math. **37**, 823-843 (1936). https://doi.org/10.2307/1968621.

6. Teslyk, M. V., Teslyk, O. M. and Zadorozhna, L. V. Quantum Logic under Semiclassical Limit: Information Loss. Ukr. J. Phys. **67**, 352-364 (2022). https://doi.org/10.15407/ujpe67.5.352.

7. Litvinov, G. L., Maslov, V. P. and Shpiz, G. B. Idempotent (Asymptotic) Mathematics and the Representation Theory. NATO Sci. Ser., Springer, Dordrecht. **77** (2002). https://doi.org/10.1007/978-94-010-0575-3_13.

8. Berthiaume, A., van Dam, W. and Laplante, S. Quantum Kolmogorov Complexity. J. Comp. Sys. Sci. **63**, 201-221 (2001). https://doi.org/10.1006/jcss.2001.1765.

Quantum correlations and magnetic properties of ultracold Fermi gases with SU(4) spin symmetry in anisotropic cubic optical lattices

Vladyslav Unukovych

V.N. Karazin Kharkiv National University, 4 Svobody Square, Kharkiv, 61000, Ukraine

Optical lattice represents itself as a spatially-periodic potential produced by coherent laser beams, where ultracold atomic gas is trapped [1]. By means of the electric field formed by the lasers, the dipole moment of atoms is induced and interacts with the field. If the frequency of lasers is adjusted close to the resonance frequency of atoms, the trapping potential can be formed due to the ac Stark effect. Thus, one can consider these systems as analogs of real crystals with neutral atoms instead of electrons. This enables the usage of optical lattices for both experimental and theoretical purposes as a tool to simulate the real crystalline materials and verify results of different models, for instance the Ising or Hubbard models.

In our research, we are mainly interested in the description of systems with high spin symmetries, specifically SU(4)-symmetric fermionic mixtures. In practice, this particular high spin symmetry can be obtained, if we choose atoms of ^{173}Yb or ^{87}Sr, and cool them down to the temperatures of the order of 1 μK. A particular choice of these is based on the unique properties of alkaline-earth-like atoms. Since fermionic isotopes of ^{173}Yb and ^{87}Sr have 6 and 10 nuclear spin projections, respectively [2], one can separate atoms with the needed amount of projections via Stern-Gerlach method. Remaining components are commonly referred to as the pseudospin flavors. The symmetry of the interaction between flavors appears due to the fact that the outer electron shell is filled, while the nuclear spin negligibly affects the interaction of the flavors.

In order to study quantum correlations and magnetic properties of SU(4)-symmetric systems, we apply the Dynamical Mean Field Theory algorithm to the Hubbard model on 3D cubic lattice. The model itself was introduced by J. Hubbard to describe the behavior of electrons in the crystals, allowing the electrons to tunnel to neighboring sites on the lattice and interact locally with each other [3]. The same model can be applied to optical lattices loaded with the atoms instead of electrons, which gives an opportunity to observe certain exotic phenomena. The Hamiltonian for SU(4)-symmetric fermionic mixture can be written as

$$H = H_t + H_U = -\sum_{\langle i,j\rangle, \sigma, \gamma} t_\gamma c^\dagger_{i\sigma} c_{j\sigma} + \frac{U}{2} \sum_{i, \sigma_1 \neq \sigma_2} n_{i\sigma_1} n_{i\sigma_2}.$$

Here $c^\dagger_{i\sigma}$, $c_{i\sigma}$ and $n_{i\sigma}$ stand for creation, annihilation and number operators of particle with the flavor $\sigma = \{1,2,3,4\}$ on the site i, respectively, meanwhile the indices of the first sum $\langle i,j\rangle$ should be regarded as the summation over all adjacent sites i and j, while γ denotes the spatial direction, e.g., $\gamma = \{x,y,z\}$. The first term represents tunneling to nearest-neighbor sites, while the second one describes two-particle interactions between flavors on the same site. Is is worth noting that the Hamiltonian itself is invariant under the action of the generators of the SU(4) symmetry.
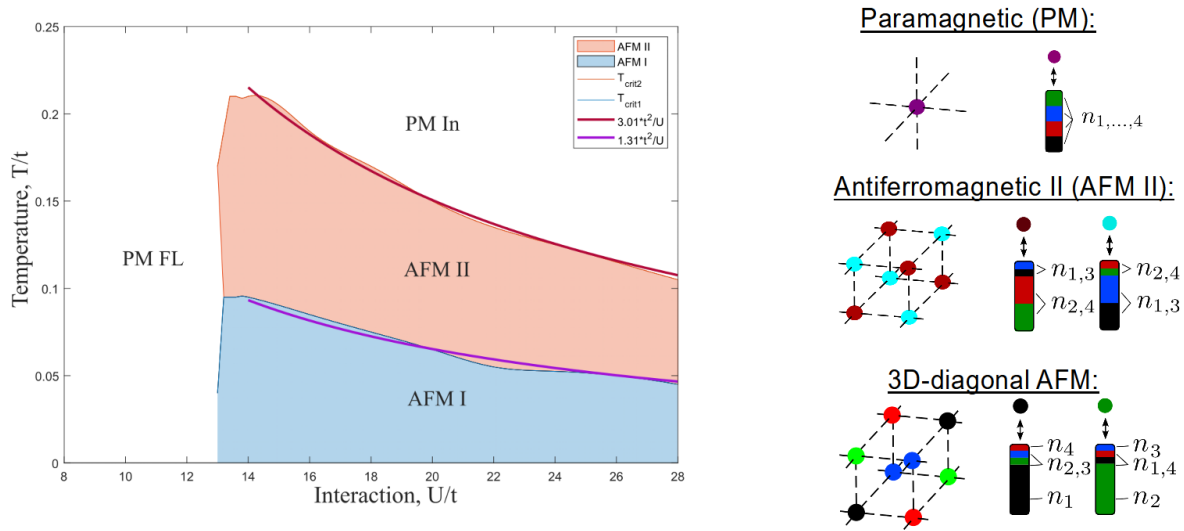
Figure 14.1: Phase diagram (left) of isotropic cubic lattice with visualization of different magnetic states (right). Each color in the bar represent the probability with which every flavor appears on the site.

Specifically, we are interested in the behavior of the system under the change of the tunneling amplitude along a specific direction [4]. For example, in a cubic lattice with three equal tunneling amplitudes related to crystallographic axes ($t_x = t_y = t_z$), we pick one amplitude (t_z) and trace how its variation affects the phase diagram. When the chosen amplitude equals to zero, the lattice splits into decoupled 2D planes. Each layer in this case have the same phase diagram as it is for a 2D square lattice. Depending on the interaction strength and temperature, the system can be in one of four different phases: a paramagnetic Fermi-liquid state in the region of small interaction amplitudes and three insulator states – one paramagnetic (PM) and two different antiferromagnetic (AFM), which experience specific type of ordering (long-range correlations), see Ref. [5] for more details.

In the opposite limit of the value of the tunable hopping amplitude ($t_z = t_{x,y}$), one can realize an isotropic cubic lattice. In this case, the phase diagram still has four magnetic phases depicted in Fig. 14.1. Despite a similarity of the diagram to the one obtained for a square lattice, with the phase transitions occurring at larger interaction amplitudes and higher temperatures, the main difference constitutes in a specific real-space modulation in the low-temperature antiferromagnetic region (AFM I). One can notice that in AFM I the cubic lattice can be divided into four sets of parallel diagonals, where each site on a diagonal has the same filling by flavors. With an increase of the temperature, this ordering breaks and only two alternating fillings of sites appear. At even higher temperature, every site becomes equivalent to any other forming the paramagnetic phase. The latter two orderings are identical to those occurring in 2D-layered lattice. It is worth noting that for the studied cases an exotic behavior takes place in the vicinity of the triple point between the Fermi-liquid phase and two antiferromagnetic phases. If the system starts in the low-temperature region, the order vanishes naturally under the heating process, as the system undergoes transition to the paramagnetic Fermi liquid, though at even higher temperature another (two-sublattice) antiferromagnetic phase emerges.
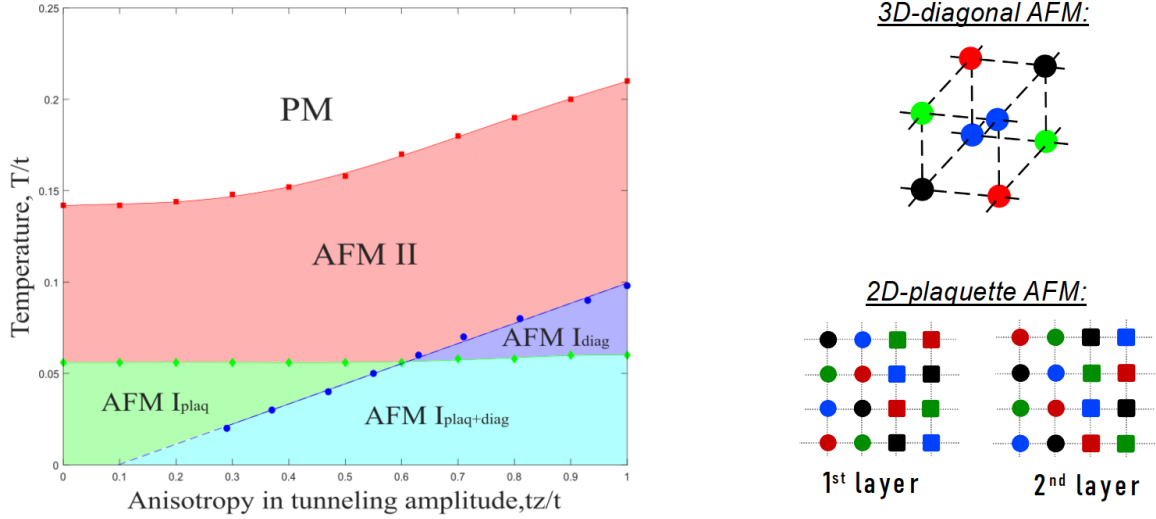
Figure 14.2: *Left side*: Phase diagram of Mott-insulator magnetic states in dependence on anisotropy of tunneling amplitude of optical lattice for amplitude of interaction $U = 14t$ ($t_x = t_y = t$). *Right side*: Visualization of 3D-diagonal (top) and 2D-plaquette (bottom) AFM orderings, where different colors represent different dominating flavor.

While both limiting cases of lattice geometries can be obtained by variation of the chosen tunneling amplitude t_z, the 3D-diagonal ordering and 2D-plaquette ordering are sizeably different and cannot be transformed into each other under a continuous transition. Hence, the discontinuity must occur at a certain value of the hopping amplitude. To answer that question, we start with isotropic cubic lattice with 3D-diagonal order and decrease the value of the chosen tunneling amplitude, until it vanishes, which shows us the region of stability of this particular magnetic ordering. Similarly, we define the region of existence of 2D-plaquette order. The combined phase diagram is presented in Fig. 14.2. The former state does not exist at any value of the anisotropy in tunneling amplitude, but only remains stable above $t_z/t \approx 0.1$. This uncertainty appears due to limitation of the Dynamical Mean Field Theory algorithm to a certain nonzero temperature. Thus, we applied the extrapolation of data in this region, which is depicted as a dashed line. Contrary to the 3D-diagonal AFM state, which boundary represented by an inclined line, the boundary of plaquette state is a horizontal line, that exists at any anisotropy and slightly increases at higher values. Hence, the region where two states coexist is depicted on the diagram. In turn, by looking at the transition to the paramagnetic Mott-insulator state, we conclude that the boundary resembles a part of a generalized hyperbola, with critical temperature remaining constant in the vicinity of zero interlayer hopping and monotonously increasing with the increase of t_z.

References

1. C. S. Chiu, G. Ji, A. Mazurenko, D. Greif, and M. Greiner, Phys. Rev. Lett. **120**, 243201 (2018).

2. C. Wu, Physics **3**, 92 (2010).

3. J. Hubbard, Proceedings of the Royal Society of London. Series A. Mathematical and Physical Sciences **276** (1365) 238–257 (1963).

4. A. Golubeva, A. Sotnikov., and W. Hofstetter, Phys. Rev. A **92**, 043623 (2015).

5. V. Unukovych, A. Sotnikov. Phys. Rev. B **104**, 245106 (2021).

Acknowledgements